

Original Research Communication

High copper complex stability and slow reduction kinetics as key parameters for improved activity, paraptosis induction and impact on drug-resistant cells of anticancer thiosemicarbazones

Sonja Hager,^{1,2§} Veronika F.S. Pape,^{3,4§} Vivien Pósa,^{5,6} Bianca Montsch,^{1,2} Lukas Uhlik,^{1,2} Gergely Szakács,^{1,3} Szilárd Tóth,³ Nikolett Jabronka,³ Bernhard K. Keppler,^{2,7} Christian R. Kowol,^{2,7} Éva A. Enyedy,^{5,6*} Petra Heffeter,^{1,2*}

¹ Institute of Cancer Research, Medical University of Vienna, Borschkegasse 8a, A-1090 Vienna, Austria

² Research Cluster 'Translational Cancer Therapy Research', A-1090 Vienna, Austria

³ Institute of Enzymology, Research Centre for Natural Sciences, Hungarian Academy of Sciences, Magyar Tudósok körútja 2, H-1117 Budapest, Hungary

⁴ Department of Physiology, Semmelweis University, Tűzoltó utca 37-47, H-1094 Budapest, Hungary

⁵ Department of Inorganic and Analytical Chemistry, Interdisciplinary Excellence Centre, University of Szeged, Dóm tér 7, H-6720 Szeged, Hungary

⁶ MTA-SZTE Lendület Functional Metal Complexes Research Group, University of Szeged, Dóm tér 7, H-6720 Szeged, Hungary

⁷ Institute of Inorganic Chemistry, Faculty of Chemistry, University of Vienna, Waehringer Str. 42, A-1090 Vienna, Austria

§ These authors contributed equally to the main findings of this manuscript.

Running title: Insights into the MoA of nM TSCs

Keywords: solution stability, thiosemicarbazones, copper complexes, protein disulfide isomerase, paraptosis, superoxide dismutase

Authors for correspondence: University of Szeged, Department of Inorganic and Analytical Chemistry, Interdisciplinary Excellence Centre, Dóm tér 7, H-6720 Szeged, Hungary. Phone: +36-62-544334. E-mail: enyedy@chem.u-szeged.hu

Medical University of Vienna, Institute of Cancer Research, Borschkeg. 8a, A-1090 Vienna, Austria. Phone: +43-1-40160-57594. Fax: +43-1-40160-957555. E-mail: petra.heffeter@meduniwien.ac.at.

Word count: 8 172 (incl. Abstract, Introduction, Results, Discussion, Materials & Methods)

References: 60

Greyscale illustrations: 4 *Color illustrations:* 1

Abstract

Aims: Due to their significant biological activity, thiosemicarbazones (TSCs) are promising candidates for anticancer therapy. In part, the efficacy of TSCs is linked to their ability to chelate essential metal ions such as copper and iron. Triapine, the best-studied anticancer TSC, has been tested clinically with promising results in hematological diseases. During the last years, a novel subclass of TSCs with improved anticancer activity was found to induce paraptosis, a recently characterized form of cell death. The aim of this study was to identify structural and chemical properties associated with anticancer activity and paraptosis induction of TSCs.

Results: When testing a panel of structurally related TSCs, compounds with nanomolar anticancer activity and paraptosis-inducing properties showed higher copper(II) complex solution stability and a slower reduction rate, which resulted in reduced redox activity. In contrast, TSCs with lower anticancer activity induced higher levels of superoxide that rapidly stimulated superoxide dismutase expression in treated cells, effectively protecting the cells from drug-induced redox stress.

Innovation: Consequently, we hypothesize that in case of close Triapine derivatives, intracellular reduction leads to rapid dissociation of intracellularly formed copper complexes. In contrast, TSCs characterized by highly stable, slowly reducible copper(II) complexes are able to reach new intracellular targets such as the ER-resident protein disulfide isomerase.

Conclusions: The additional modes of actions observed with highly active TSC derivatives are based on intracellular formation of stable copper complexes, offering a new approach to combat (drug-resistant) cancer cells.

Introduction

Thiosemicarbazones (TSCs) possess significant biological activity, which resulted in their development as pharmaceuticals against several diseases, including cancer (24). In part, the efficacy of TSCs is linked to their ability to chelate essential metal ions such as copper and iron. Cancer cells, in particular, require higher amounts of these metal ions due to their increased rate of replication (3,60). As a result, the ability of α -N-heterocyclic TSCs to form stable metal complexes is an important property for their development as anticancer agents (26).

Initially, the mechanism of action of α -N-heterocyclic TSCs was thought to primarily rely on the depletion of iron and the consequential inhibition of the iron-containing enzyme ribonucleotide reductase (57). However, the role of other metals (especially copper), metalloenzymes and metal-interacting proteins is gaining more attention (16,22). For example, the ability of copper(II)-TSC complexes to undergo redox cycling in the presence of reducing agents, with production of reactive oxygen species (ROS) (a process also called "activation by reduction" (22)), and the disruption of the cellular thiol redox homeostasis is increasingly discussed as relevant contributions to TSC activity (11,23,27,44). Furthermore, the interaction with copper ions has been recently suggested to be involved in collateral sensitivity of P-glycoprotein (P-gp, ABCB1)-overexpressing multidrug-resistant cancer cells to the nanomolar-active TSC di-2-pyridylketone 4,4-dimethyl-3-thiosemicarbazone (Dp44mT) (21). Interestingly, recently performed studies confirmed the enhanced sensitivity of certain P-gp-overexpressing cells (e.g. MES-SA/Dx5) to several metal chelators (including Dp44mT), but also suggested that the collateral sensitivity of these MDR cells may rely on other (more complex) mechanisms independent of P-gp transport function (9,40).

With regard to the clinical situation, the best studied anticancer TSC, Triapine, has been already tested in several phase I and II trials with promising results especially against hematological diseases (12,25,54,56,59). Currently, this drug is being investigated as chemo- and radiosensitizer in an ongoing clinical phase III study assessing Triapine in combination with cisplatin and radiation therapy (NCT02466971) (30). In addition, two other α -N-heterocyclic TSCs di-2-pyridylketone 4-cyclohexyl-4-methyl-3-thiosemicarbazone (DpC) and 4-(pyridine-2-yl)-N-[[8E)-5,6,7,8-tetrahydroquinolin-8-

ylidene]amino}}piperazine-1-carbothioamide (Coti-2) recently entered clinical phase I trials (www.clinicaltrials.gov). Noteworthy, these two compounds as well as Dp44mT (the predecessor of DpC) and our dimethylated Triapine derivative Me₂NNMe₂ represent a subclass of TSCs characterized by a ~500-fold higher anticancer activity compared to Triapine in cell culture (20,37). Recent studies suggested that this efficiency could be based on an additional mode-of-action, associated with the formation of intracellular copper complexes (16,19,34). In particular, our group discovered that these compounds are able to induce paraptosis, a novel form of programmed cell death (13). Paraptosis is a caspase-independent cell death discernable by the appearance of cytoplasmic vesicles originating from the endoplasmic reticulum (ER) (33,50). TSC-induced paraptosis appears to be associated with the (copper-dependent) inhibition of the ER-resident protein disulfide isomerase (PDI) (13). In light of these recent data, the aim of this study was to elucidate the role of copper complex formation of various TSCs in anticancer activity, paraptosis induction and collateral sensitivity. For this purpose, we investigated solution stability and redox properties of a selected panel of structurally related α -N-heterocyclic TSCs and their respective copper(II) complexes. The measured physico-chemical properties were then correlated with biological parameters (anticancer activity, resistance ratio of multidrug-resistant (MDR) cancer cells, paraptosis induction and PDI inhibition). Thus, we show that highly active TSCs (with IC₅₀ values in the nanomolar range) form copper(II) complexes characterized by high stability and slow reduction kinetics. Our data suggest that these stability and redox properties protect the copper(II) complexes of this TSC subclass from premature reduction-induced ligand liberation allowing the interaction of the copper(II) complexes with intracellular targets such as the ER-resident PDI. In contrast, the copper complexes of TSCs such as Triapine are sensitive to rapid reduction and thus ligand liberation inside the cancer cells, which are efficiently protected from the generated superoxide by the upregulated enzyme superoxide dismutase (SOD) in cell culture as well as in a tumor model in vivo.

This paper has been peer-reviewed and accepted for publication, but has yet to undergo copyediting and proof correction. The final published version may differ from this proof.

High copper complex stability and slow reduction kinetics as key parameters for improved activity, paraptosis induction and impact on drug-resistant cells of anticancer thiosemicarbazones (DOI:

Antioxidants and Redox Signaling

10.1089/ars.2019.7854)

Results

Anticancer activity and paraptosis-inducing potential of the TSC panel

As a first step, the *in vitro* anticancer activity of the selected α -*N*-pyridyl TSCs (see Table 1 for their chemical formulae) and their preformed (i.e. in situ generated) copper(II) complexes (in a 1:1 metal-to-ligand ratio) was measured in human colon adenocarcinoma SW480 and uterine sarcoma MES-SA cells as well as the multidrug-resistant subline MES-SA/Dx5. SW480 cells were investigated by conventional MTT assay, while the fluorescently labelled MES-SA and MES-SA/Dx5 cells were tested in co-culture using an automated system (Figure 1A and B, Table 1 and 2 as well as Suppl. Table 1 - 4) (55). In accordance to previous reports (27-29,47,52), following 72 or 144 h incubation, the three terminally dimethylated compounds pyridine-2-carbaldehyde thiosemicarbazone (PTSC), Me₂NNMe₂, Dp44mT and the disubstituted derivative DpC showed distinctly higher anticancer activities than the other compounds (2-formylpyridine thiosemicarbazone (FTSC), Triapine, H₂NNHMe, H₂NNMe₂, MeHNNMe₂, Me₂NNH₂, Me₂NNHMe). This was especially pronounced in the MES-SA/Dx5 cell model, reflecting the collateral sensitivity of the P-gp-overexpressing cells to this subtype of TSCs (Table 1 and 2, Figure 1B).

In order to gain more insight into the time dependency of these effects, the activity of the compounds was also assessed after 3 and 24 h. None of the metal-free ligands exhibited relevant anticancer activity after 3 h resulting in IC₅₀ values above the highest tested concentration of 25 μ M. With the exception of PTSC, Dp44mT and DpC, the compounds did not decrease viability following a 24 h-long incubation with the tested cancer cells. Interestingly, in contrast to the later time points (Figure 1B), collateral sensitivity of MES-SA/Dx5 cells was not observed at 24 h (Suppl. Table 2 and 3), indicating that the collateral sensitivity might be based on enhanced cell cycle arrest rather than enhanced apoptosis. The anticancer activity of copper(II) complexes was slightly different (Table 1 and 2 as well as Suppl. Table 1 - 4). Several complexes were already active after a relatively short incubation time (24 h) in SW480 cells (Suppl. Table 1 - 3), showing the same activity pattern as observed in the 72 h experiment (Table 1). However, after 72 h IC₅₀ values of all tested copper complexes were in a similar range as the respective metal-free ligands (Figure 1A, Table 1), with the exception of Me₂NNHMe, which was significantly more active

as a copper(II) complex. Thus, the long-term anticancer activity of the copper complexes of the nanomolar-active TSCs was similar to that of the respective metal-free ligand.

In order to investigate the paraptosis-inducing potential of the compounds, perinuclear vesicle formation was investigated by microscopy after drug treatment (Figure 1C). In agreement with previous results (13), Me₂NNMe₂, Dp44mT and DpC induced high levels of vacuolization in SW480 cells already at 0.1 μM drug concentrations (Figure 1C and D). In addition, also incubation with the terminally dimethylated PTSC, H₂NNMe₂ and MeHNNMe₂ likewise induced paraptosis (however, vacuolization at 0.1 μM was observed only in case of PTSC, while for the other two derivatives, the effect was visible only at 1 μM, reflecting their higher IC₅₀ values). Similar results were obtained in MES-SA cells (Suppl. Figure 2).

Proton dissociation processes and pK_a values of the investigated TSCs

As there is a distinct structure-activity relationship in our TSCs panel, subsequently, we characterized whether these effects are reflected by differences in their chemical properties. While for Triapine and some derivatives several reports on proton dissociation processes are available (5-7), for most of the compounds in this study this parameter has not been characterized so far (especially not in pure aqueous solution). First, pK_a values were determined by UV-visible (UV-vis) spectrophotometric titrations in pure water at compound concentrations of 10-50 μM. In case of DpC, addition of some dimethyl sulfoxide (DMSO) was necessary and the pK_a values of DpC in pure water were estimated by extrapolation (Table 3; Suppl. Figure 3A). For all compounds, the measured UV-vis spectra revealed characteristic changes upon increasing pH, as it is depicted exemplarily for Me₂NNMe₂ in Figure 2A. The pH-dependence of the absorbance values always showed two well-separated deprotonation steps: one at pH 2.5–6.0 and one at 8.0-11.5. Therefore, two pK_a values could be determined (Table 3). The λ_{max} and ε values of the ligand species in the different protonation states are collected in Suppl. Table 5. The calculated individual spectra (*e.g.* for Me₂NNMe₂ in Suppl. Figure 3B) represent significant differences between the molar absorptivities of the various ligand species (Suppl. Table 5). Notably, the pK_a of the second pyridyl moiety in Dp44mT and DpC could not be determined under the applied conditions due to its fairly acidic character. Analysis of the pK_a values revealed that *N*-terminal dimethylation results in slightly higher pK_a (H₂L⁺) and lower pK_a (HL) (Triapine vs.

H₂NNMe₂ or FTSC vs. PTSC etc.), whereas dimethylation of the pyridine amine increases slightly both pK_a values (Triapine vs. Me₂NNH₂). At the same time monomethylations have only a minor influence. The dipyridyl derivatives Dp44mT, DpC as well as FTSC and PTSC possess decreased pK_a H₂L⁺ by almost one order of magnitude, but no clear trend was evident for pK_a HL. In general, not only the electron-donating/withdrawing properties of the substituents should be considered to explain differences in pK_a values, but also the ability of the derivatives to be stabilized by mesomeric/resonance effects (e.g. the thione/thiol equilibrium). As apparent from the determined pK_a values all TSCs investigated in this study are charge neutral (in HL form) at physiological pH.

High copper(II) complex solution stability is an important parameter for anticancer activity

Having characterized the (de)protonation behavior of our TSCs, we evaluated the stability of the respective copper complexes in aqueous solution. Based on our previous findings (5,6), we assumed that some of the studied α -N-pyridyl TSCs (Triapine, FTSC, PTSC, H₂NNMe₂) form very stable [CuL]⁺ complexes in a wide pH range. At lower pH, the balance shifts to [CuLH]²⁺ complexes, containing the protonated ligand. In contrast, a mixed hydroxido complex [CuL(OH)] is prevalent in the basic pH range, while at ligand excess further species (e.g. [CuL₂], [Cu₂L₃]⁺) can be found (6).

Equimolar aqueous solutions of the metal ion and the respective ligands (10 or 25 μ M concentration) were titrated and the deprotonation processes of the complexes were followed spectrophotometrically (Figure 2B for Cu-Me₂NNH₂). Deconvolution of the spectra resulted in the pK_a values of the copper(II) complexes and their individual absorbance spectra (Suppl. Table 6, Suppl. Figure 3C). All pK_a values were in the range of 2.1-2.6 (for [CuLH]²⁺) and 8.1-8.8 (for [CuL]⁺) and thus well comparable to reported data of FTSC (with 1% DMSO) (1). In general, the pK_a value of [CuLH]²⁺ was by 7.2-8.6 orders of magnitude lower compared to that of the metal-free HL form, revealing that displacement of the dissociable proton in the complex is mediated by the metal ion coordination. As the formation of the complex [CuL]⁺ is predominant in a wide pH range (4–6.5) (Figure 2C for Cu-Triapine) and assumed to be quantitative due to the high solution stability, apparent (conditional) formation constants (β') for this type of complexes were subsequently determined by competition experiments with EDTA (24) (Figure 2D for 1:1 Cu-Me₂NNHMe

and Suppl. Figure 3D). Since the displacement was found to be relatively slow, 1–2 h equilibration time was applied for this reaction (the reverse experiment using Cu-EDTA + FTSC resulted in the same endpoint; see Suppl. Figure 4). Increasing amounts of EDTA resulted in decreasing absorbance at the wavelength characteristic for the S→Cu charge transfer band (*e.g.* 422 nm in case of Me₂NNHMe in Figure 2D). Taken into account the conditional stability constants determined (Suppl. Table 6) as well as the proton dissociation constants of the ligands (Table 3), the overall stability constants (β) of the complexes [CuL]⁺ were calculated (Table 3). Furthermore, also the β values of the other two types of complexes [CuLH]²⁺ and [CuL(OH)] were computed (Table 3) using the pK_a of [CuLH]²⁺ and [CuL]⁺ (Suppl. Table 6). Based on these data, it can be concluded that at physiological pH, [CuL]⁺ is the most predominant species, accompanied by a smaller fraction (3.9-16.3%) of [CuL(OH)] (Table 3, Figure 2C).

Since a direct comparison of the log β [CuL]⁺ constants is not adequate due to the different basicity of the ligands, pCu (–log [Cu(II)]) values were calculated in order to compare the copper(II)-binding ability of the studied TSCs at pH 7.4 (a higher pCu value indicates a stronger metal ion-binding ability of the ligand) (Table 3). The calculated pCu values revealed that dimethylation at both the terminal and the pyridine amino group increased complex stability. On the contrary, the effect of monomethylation on the copper(II)-binding ability was minor at both positions. Undoubtedly, the four compounds with activity in the nanomolar range form copper(II) complexes with the highest stability, followed by the two trimethylated compounds MeHNNMe₂ and Me₂NNHMe and all other derivatives (Table 3).

To evaluate the effect of copper complex stability on the biological activity, the pCu and 72 h pIC₅₀ values of either the ligands or their *in situ* generated copper complexes were correlated. These analyses revealed that the ligands with high pIC₅₀ values possess a higher copper(II)-binding ability (indicated by higher pCu values) and the correlation is even more pronounced for the pIC₅₀ values of the copper(II) complexes (Figure 2E and Suppl. Figure 4). Accordingly, the higher copper complex stability was also associated with higher activity in the multidrug-resistant cells after long-term incubations (Figure 2F) and paraptosis induction (Figure 2G), indicating an important role of the copper(II) complex in these TSC-induced effects.

Reduced reduction rate of copper(II) complex has a strong impact on TSC activity

In addition to the stability of the formed copper(II) complexes, also their redox properties may have an impact on their biological activities. In order to investigate, whether there are differences in the reduction rates of our TSC panel, the redox reactions of the *in-situ* generated copper(II) complexes with two physiological reducing agents, namely ascorbic acid (AA) and L-glutathione (GSH), were studied. Reduction of the copper(II) complexes was followed spectrophotometrically in aqueous solution at pH 7.4 under anaerobic conditions.

In good agreement with the literature (11), no time-dependent spectral changes were observed in the case of AA which suggests that these metal complexes cannot be reduced by AA under the applied conditions (see Suppl. Figure 5). This could be explained by the relatively weak reducing power of ascorbate (formal potential at pH 7.4: +0.05 V for dehydro-L-ascorbate/AA) (15). In contrast, the stronger reducing agent GSH (formal potential at pH 7.4: -0.26 V for GSSG/GSH (45) reduced all studied copper(II) TSC complexes, although with different rates (Figure 3A and B).

The first recorded spectrum after mixing the reactants showed a small shift of the λ_{\max} value (e.g. 448 \rightarrow 452 nm, as shown for Cu-MeHNNMe₂ in Figure 3A) most probably due to the formation of a mixed ligand complex with GSH, as it is reported for various TSC complexes (22,44). This shift was followed by a significant decrease of the absorbance at this λ_{\max} , while the absorbance value at the λ_{\max} of the free ligand (~382 nm) increased, probably as a result of the decomposition of the generated unstable copper(I) complex. Noteworthy, oxygenizing (bubbling O₂ into) the solution regenerated the original copper(II) complexes, confirming the reversibility of the redox process (data not shown). The other studied TSCs behaved similarly. However, significant differences were observed regarding the reduction rates of the respective complexes (Figure 3B). In order to obtain comparable data, the recorded absorbance/time curves were further analyzed at the λ_{\max} of the complexes. The calculated k_{obs} , half-lives ($t_{1/2}$) and percentage of non-reduced complex after 1 h in the presence of 50 equiv. (1.25 mM) of GSH are collected in Table 4. For selected complexes (Triapine, PTSC), kinetic runs were additionally performed at other equivalents of GSH, and k_{obs} were found to be very sensitive to the concentration of the reducing agent, namely slower reaction rates with decreasing excess of GSH were

observed (data not shown). In accordance to the reports from Santoro et al. (44) under the applied conditions, the reduction of the copper(II) complexes was incomplete, especially with nanomolar-active compounds (see plateau in Figure 3B and % non-reduced copper(II) complex after 1 h in Table 4). Interestingly, the remaining fraction of non-reduced copper(II) complex after 1 h (Table 4) showed a strong correlation with the pCu value and, therefore, with the solution stability of the copper(II) complexes (Figure 3C). These data demonstrate that the copper(II) complexes of α -*N*-pyridyl TSC ligands bearing higher solution stability can only be reduced by GSH in a slower and much less effective way. When these reduction rates were subsequently correlated with the anticancer activity (after 72 h), it became apparent that a slower reduction rate is associated with higher anticancer activity (Figure 3D and Suppl. Figure 6A) and paraptosis-inducing potential (Figure 3E and Suppl. Figure 6B) of the metal-free ligands as well as the copper complexes. Overall, these results are surprising, as so far it has been assumed that the anticancer activity of copper TSC complexes is mainly based on intracellular redox activity, either by the copper(II) TSC itself or by the copper release from the complex in the cell (22,44).

Copper(II) complex stability influences redox behavior of TSCs under cell-free conditions

It is widely accepted in the literature (22,27,38,44), that reduction of copper(II) complexes to copper(I) and their subsequent re-oxidation under aerobic conditions, results in the generation of superoxide radicals and thus redox stress in treated cells. In order to compare the obtained reduction rates of the copper(II) complexes by GSH to their superoxide production potential, formation of cell-free superoxide was measured spectrophotometrically using the nitroblue tetrazolium (NBT) assay. In line with the activation by reduction theory for this compound class (16), without the addition of a reducing agent, none of the tested TSCs (neither as metal-free ligand nor as copper(II) complex) induced any positive signal (data not shown). In contrast, as expected when the GSH precursor and reducing agent *N*-acetyl cysteine (NAC) was added to the copper(II) complexes, superoxide generation (up to 1.6-fold compared to the control) was detected (Figure 3F). In agreement with the above shown results, distinct differences between the individual ligands were observed. Thus, indeed copper(II) complexes with a higher stability and slower reduction rate produced also less cell-free superoxide (Figure 3G and Suppl. Figure 7). In contrast, copper ions, which under certain conditions have been reported to

induce ROS on their own (10,41), did not result in positive measurable NBT signals (at 5 μM) neither alone nor in combination with NAC (data not shown). Consequently, these data indicate that despite the widely accepted hypothesis that the anticancer activity of copper(II) complexes is based on (intracellular) reduction-induced ROS (superoxide) formation, in our hands especially the TSC complexes showing reduced redox activity are characterized by distinctly enhanced cytotoxicity.

Stimulation of antioxidant enzymes and stress-response genes in TSC-treated cells

In order to investigate, whether we can also detect superoxide production upon drug treatment in living tumor cells, the dihydroethidium (DHE) assay was used at conditions similar to the cell-free assay. Comparably to the results of the cell-free experiments, neither the ligands nor copper ions (5 μM) alone did significantly increase the fluorescence signals (data not shown). Unexpectedly, for the copper(II) complexes a different picture emerged compared to the cell-free experiments, as no significant increase in superoxide levels could be detected neither in presence nor in absence of NAC (Figure 4A). Hypothesizing that cancer cells efficiently protect themselves from TSC-induced redox stress by upregulation of antioxidant response signaling, we used our previously published (13) whole genome gene expression data of Triapine- and Me_2NNMe_2 -treated SW480 cells. In these experiments cells were treated either with Triapine (1 μM), Me_2NNMe_2 (0.1 and 1 μM) or solvent for 15 h and mRNA levels were analyzed for drug-induced changes in gene transcription. When looking for altered gene sets associated with response to oxidative stress (e.g. “regulation of response to oxidative stress”) by gene set enrichment analysis (GSEA), no significant gene set enrichment was detected (lowest FDR values: 0.10 for Me_2NNMe_2 and 0.35 for Triapine (Suppl. Figure 8)). However, when looking at individual genes, we found upregulation of the superoxide scavenger enzymes SOD2 and SOD3, but not SOD 1 upon Triapine treatment (Figure 4B). In contrast, in Me_2NNMe_2 -treated cells no comparable upregulation was observed for SOD2 (at IC_{50} concentrations) and SOD3 (Figure 4B).

For confirmation at the protein level, Western blot analysis of SOD2 with lysates from cells treated with our TSC panel were performed. Indeed, SOD2 was upregulated after treatment with Triapine and all other micromolar-active TSCs, while none of the compounds with activity in the nanomolar concentration range induced SOD2 expression

(Figure 4C and D). To test whether SOD2 was also upregulated by Triapine treatment in tumor cells in vivo, CT-26 colon carcinoma-bearing mice were treated orally with either solvent or 10 mg/kg Triapine. As shown in Supp. Figure 10, Triapine had significant anticancer activity and was well tolerated in this setting. On the last day of treatment (day 15), the tumors were collected and immunohistochemically stained for SOD2. In accordance with the array data as well as the Western blot analysis, also tumors from Triapine-treated animals showed strong stimulation of SOD2 expression compared to the solvent control (Figure 4E).

Overall, the significant upregulation of SOD is in line with the hypothesis of efficient degradation of TSC-induced ROS and might explain the discrepancy of superoxide production between the cell-free and cell culture experiments observed above. Despite its much higher cytotoxicity, the SOD stimulation was weaker in case of Me_2NNMe_2 and the nanomolar-active TSCs, indicating that (in contrast to Triapine) at drug doses in the IC_{50} range no significant generation of superoxide occurs in the treated cells with these compounds. Consequently, it can be hypothesized that due to the higher resistance of the copper(II) complexes towards reduction, the compounds are less efficient in ROS production inside of cells.

Based on the assumed importance of metal chelation in the mode of action of TSCs, we also investigated changes in pathways regarding metal homeostasis in our arrays. Interestingly, we found only one significantly changed gene set, namely upregulation of genes involved in “response to zinc ions” after treatment with Me_2NNMe_2 (Figure 4F). This is of interest, as a closer look on this gene set revealed that, this gene set mainly contains metallothioneins (which are cysteine-rich, low molecular weight proteins being responsible also for copper homeostasis) as well as the copper transporters ATP7A and ATP7B (Figure 4G).

High copper complex stability is important for PDI inhibition potential

In a previous study, we showed that Me_2NNMe_2 induces paraptosis by inhibition of the ER-resident PDI and consequent disruption of the ER thiol redox homeostasis (13). Therefore, the here studied copper-TSC complexes were tested for their potential to inhibit this enzyme. In line with our previous report (13), copper in form of a simple salt was already able to inhibit the PDI enzymes to some extent. This inhibition distinctly increased when

copper was complexed by Me_2NNMe_2 or other TSCs with terminal dimethylation/di-substitution (Figure 5A). Interestingly, the inhibition followed an “all-or-nothing” pattern with complexes showing either the same weak inhibition as copper ions alone or strong PDI-disrupting ability comparable to the Me_2NNMe_2 complex. Dividing the compounds in these two categories, it can be clearly seen that PDI inhibition is associated with higher complex stability, higher anticancer activity and enhanced vesicle formation (Figure 5B and Suppl. Figure 11). Thus, although inhibition of the PDI is probably not the only target of the nanomolar-active TSCs (other targets may include the ribonucleotide reductase (RR) inhibition) (29,58), this indicates that there is a link between redox properties and copper complex stability with PDI inhibition and paraptosis induction, which needs to be further investigated in future studies.

Discussion

TSCs have long been known for their anticancer activity and their metal-chelating abilities (16,23). In case of the currently in phase III clinically investigated derivative Triapine, especially an interaction with the iron homeostasis was suggested based on its strong inhibition of the iron-containing ribonucleotide reductase and the occurrence of methemoglobinemia as the main adverse effect in patients (16). With the aim to develop TSCs with improved efficiency, derivatives with activity in the nanomolar IC_{50} range (such as DpC, Dp44mT and Me_2NNMe_2) came into the focus of interest during the last decade of which DpC also recently entered clinical trials (2,20,28,29). An increasing body of evidence indicates that these drugs have additional modes of action that are responsible for their increased cytotoxicity. The particularities of nanomolar-active TSC are indicated by the induction of 1) a specific form of ER stress associated with disruption of the ER thiol redox homeostasis and inhibition of the ER protein PDI (13,14,39,53), 2) a just recently discovered form of programmed cell death called paraptosis (13), and 3) increased activity in some multidrug-resistant cancer cells (9,40,46). Significantly, for all of these effects, the interactions with (intracellular) copper pools leading to formation of redox-active copper complexes were suggested to be crucial (16,19,34). Thus, it was proposed that copper complexes induce ROS (superoxide) by redox reaction with intracellular reductants, a mechanism also referred to as “activation by reduction” (11,34,36,44,49). Accordingly, a strong synergism between the metal-free ligand and free copper salts has been repeatedly

reported for nanomolar-active TSCs (19,28,49). However, the experiments supporting the ROS model were often performed either with preformed copper(II) complexes (11,34) or by preincubation of the ligands with high levels of extracellular copper (28,36,49). In contrast, in many cases, incubation with the metal-free ligands alone did not induce global ROS detectable for example by the DCF-DA stain (13,28,34). Thus, it might be hypothesized that, although there are indications that copper plays an important role in the mode of action of nanomolar-active TSCs, under physiological conditions, this might not be due to reductant-induced global redox stress production. However, localized and slower non-ROS-producing redox reactions (e.g. formation of disulfide bridges) might still be involved in their activity.

The aim of this study was to further investigate the role of copper in the activity of nanomolar-active TSCs in comparison to micromolar-active derivatives such as Triapine. To this end, a selected panel of structurally related α -N-heterocyclic TSCs and their respective copper(II) complexes was investigated with regard to solution stability, cell-free as well as intracellular redox properties, toxicity against sensitive and MDR cancer cell lines and paraptosis-inducing potential. We show that the activity of the compounds has a strong correlation with these properties, confirming the relevance of their interaction with copper ions (Figure 5C).

To analyze the interaction of the compounds with copper in more detail, we compared the anticancer activity of the preformed copper complexes with that of the metal-free ligands, together with their potential to induce collateral sensitivity in a P-gp-overexpressing cell model. Thereby, crucial differences were observed between short- and long-term drug incubation. While short incubation times (3 and 24 h) resulted in higher anticancer activity for especially nanomolar-active TSC copper(II) complexes compared to metal-free ligands, after longer incubation times (72 and 144 h), mostly no enhanced efficiency of the copper complexes was observed. The increased activity is in line with the literature showing (mainly for the nanomolar-active compounds) an enhanced activity of the metal-free ligands when co-applied with an excess of simple copper salts (19,28,49) or of preformed 1:1 or 1:2 copper(II):Dp44mT complexes compared to the metal-free ligand (20). An exception to the increased activity were copper(II) complexes of Triapine, H₂NNHMe and H₂NNMe₂, which showed no activity after short-time and even lower activity compared to

the metal-free ligand after long-term incubation. This may be explained by a less efficient absorption and cellular uptake of the charged $[\text{CuL}]^+$ species compared to the neutral HL ligand which are the predominating forms in solution at physiological pH based on our solution speciation studies in all cases. After longer incubation times, the differences in activity between the copper(II) complexes and the respective metal-free ligands disappeared which could be explained by the hypothesis of different kinetics of the underlying cell killing mechanisms as described by Ishiguro *et al.* (19). Thus, while the rapid cell killing mechanism is conducted by extracellular TSC copper complexes and characterized by redox reactions (27), the slow activity is redox-independent and depends more on the ligand and/or intracellular copper complexation. In this regard, MES-SA/Dx5 cells were found to be more resistant against the rapid cell killing mechanism of both the metal-free ligands and preformed complexes compared to the parental MES-SA cells (seen in the 24 h IC_{50} values), while they were (slightly) more sensitive to the long-term activity of most copper complexes compared to the respective ligands. The exception were complexes of TSCs such as Triapine, H_2NNMeH and H_2NNMe_2 , with lower activity compared to metal-free ligands, that also did not exhibit increased activity in MES-SA/Dx5 cells as either ligand or complex. In fact, collateral sensitivity of MES-SA/Dx5 cells correlated with higher copper(II) complex stability, which further points to the importance of copper chelation for nanomolar TSC activity. This is in good agreement with previous studies, as also P-gp-overexpressing and Triapine-resistant SW480 or colchicine-resistant KB-3-1 cells showed no cross-resistance against terminally or pyridine amino di-substituted (especially nanomolar) TSCs after long-term incubation (28,52).

It is important to note that the copper(II) complexes of the studied TSC ligands have the same composition ($[\text{CuL}]^+$) with the same coordination mode ($\text{N}_{\text{pyridyl}}, \text{N}, \text{S}^-(\text{H}_2\text{O})$) at pH 7.4 in aqueous solution. However, significant differences were seen regarding their stability. Namely, the nanomolar-active TSCs form complexes of significantly higher stability with this metal ion compared to the micromolar compounds. On the other hand, the copper(II) complexes of the nanomolar TSCs could be reduced by GSH in a much slower redox reaction. When we investigated the role of redox activity, opposing to the current theory of activation by reduction (16,20,27), nanomolar-active TSCs were characterized by copper(II) complexes with higher stability and less efficient reduction by reducing agents.

This observation is in line with other studies such as from Garcia-Tojal *et al.*, and from Santoro *et al.* who both found slower reduction by GSH in the case of the copper(II) complex of Dp44mT, as compared to the copper(II) complexes of Triapine and FTSC/PTSC (11,44). Moreover, for both Triapine as well as FTSC, reduction of the copper(II) complex resulted in efficient binding of the copper(I) ion to GSH leaving a metal-free ligand able to interact with other metal ions such as iron or zinc (44). In agreement with a slower reduction, also cell-free superoxide production (which results from re-oxidation of the copper(I) complex) was lower with these complexes. Interestingly, the confirmation of these data in living cells turned out to be difficult. Thus, at physiologically relevant conditions, none of the TSC complexes increased DHE fluorescence (indicating intracellular superoxide) neither in presence of a thiol-containing reducing agent (NAC) nor in its absence. Consequently, we hypothesized that cells rapidly adapt to redox stress and efficiently degrade the drug-generated superoxide.

In line with a higher, cell-free superoxide production of Triapine and its closest (micromolar-active) derivatives, upregulation of the superoxide-degrading enzymes SOD2/3 on mRNA and protein levels was identified as a possible protection mechanism. This is of interest as comparable upregulation and increased activity of SOD enzymes was also reported and shown to protect against treatment with TSC copper complexes by other groups (11,48,51). This stimulation of SODs only in case of micromolar-active TSCs led us to the theory that in case of Triapine and its close derivatives, the rather fast (intracellular) reduction leads to rapid dissociation of the copper complex and thus liberation of the metal-free ligands (which is also in good agreement with the very recently published data of Santoro *et al.* (44)). Consequently, metal-free (or iron-/zinc-bound) Triapine could be the main species occurring inside the cell, playing a primary role in anticancer activity. In contrast, as copper(II) complexes of nanomolar-active TSCs are much slower in their reduction and thus more stable, the copper(II) complex is able to reach intracellular targets such as the ER-resident protein PDI (Figure 5D). In line with this hypothesis, paraptosis induction, measured by vacuole formation, was most pronounced with the nanomolar-active TSCs. This increase in paraptosis induction also correlated with the solution stability of their copper complexes as well as a slower reduction rate. In addition,

also PDI inhibition by the TSC complexes highly correlated with copper complex stability and vacuole formation.

In line with a more pronounced role of copper in the anticancer activity of nanomolar-active TSCs, our array analysis revealed that Me_2NNMe_2 induces upregulation of metallothioneins, which strongly bind diverse metal ions including copper(I). Noteworthy, metallothioneins also contain multiple thiol groups, and thus take part in the cellular thiol redox homeostasis (43), which seems to be disrupted by the nanomolar-active TSC copper complexes (13). Interestingly, it has been suggested by Santoro *et al.* that metallothioneins play a crucial role in the removal of the reduced copper(I) from Triapine and FTSC after reduction, while in case of Dp44mT the interaction of zinc-loaded metallothioneins with the copper(I)-TSC-GSH complex resulted in zinc transmetalation (44). In accordance, also our data indicate that there might be an interaction with metallothioneins also in the cytosol (but not in the ER) of living cells after treatment with the metal-free TSC ligand. The exact nature of this interaction definitely warrants further investigations.

Innovation (100 words)

In conclusion, the here presented work on the one hand, confirms that interaction with copper ions plays an important role in the anticancer activity of nanomolar-active TSCs. On the other hand, it also raises strong doubts on the dogma of “activation by reduction”-induced redox stress via superoxide production as main executor of (metal-free applied) drug effectivity. In contrast, we propose that due to their high solution stability, copper(II) complexes of nanomolar-active TSCs are able to reach additional intracellular protein targets such as the ER-resident PDI resulting in paraptotic cell death induction and increased anticancer activity.

Materials and Methods

Chemicals

FTSC, PTSC, Triapine, H_2NNHMe , H_2NNMe_2 , MeHNNMe_2 , Me_2NNH_2 , Me_2NNHMe , Me_2NNMe_2 , FTSC, MeHNNH_2 , MeHNNHMe , Dp44mT and DpC were prepared as described previously (28,29,35). Ethylenediaminetetraacetic acid (EDTA), KCl, KOH, HCl was obtained from Reanal (Hungary), 2-(*N*-morpholino)ethanesulfonic acid (MES) and 4-(2-hydroxyethyl)-1-piperazineethanesulfonic acid (HEPES) was purchased from Sigma-Aldrich

and used without further purification. Copper(II) stock solution was prepared by the dissolution of CuCl_2 in water and its concentration was determined by complexometry with EDTA. For cell culture experiments TSCs were first diluted in DMSO (10 mM) after which further dilutions were performed in aqueous solutions (double distilled (dd) H_2O , buffer or cell culture media depending on the assay) or with which copper complexes were formed in combination with CuCl_2 (10 mM in dd H_2O). Thereby, concentrations of DMSO in cell culture did not reach toxic doses. For spectrophotometric measurements, TSCs were directly diluted in dd H_2O at low concentrations (255 μM) and dissolution was improved by ultrasound bath and adding low concentration of HCl.

Spectrophotometric titrations

A Hewlett Packard 8452A diode array spectrophotometer was used to record the UV-Vis spectra in the interval 200–800 nm. The path length was 1 cm. Proton dissociation constants (pK_a) of the TSC ligands, the copper(II) mono complexes and the individual spectra of the species in the various protonation states were calculated by the computer program PSEQUAD (31). Spectrophotometric titrations were performed on samples containing the ligands at 10-50 μM concentration by a KOH solution in the presence of 0.1 M KCl at 25.0 ± 0.1 °C in the pH range from 2 to 11.9. An Orion 710A pH-meter equipped with a Metrohm combined electrode (type 6.0234.100) and a Metrohm 665 Dosimat burette were used for the pH-metric titrations. The electrode system was calibrated to the $\text{pH} = -\log[\text{H}^+]$ scale by means of blank titrations (HCl vs. KOH) according to the method suggested by Irving *et al.* (18). The average water ionization constant (pK_w) is 13.76 ± 0.05 in water. Argon was also passed over the solutions during the titrations.

Due to the limited water solubility of DpC pK_a values of the ligand were determined in 5 and 30% (w/w) DMSO/ H_2O solvent mixture, while pK_a values of the copper(II) complexes in 30% (w/w) DMSO/ H_2O . The pK_a values obtained at various DMSO content were plotted against the $1/\epsilon_r$ values of the solvent medium, where ϵ_r is the relative permittivity (or dielectric constant) of the solvent medium and values for the pure aqueous solution were obtained by extrapolation. The ϵ_r values are interpolated data taken from (4). Namely, the pK_a values for DpC in pure water were extrapolated from the values obtained in the DMSO/ H_2O mixtures with the slopes of the linear curves of DpC (5%, 30%), Triapine (0%, 30%) and H_2NNMe_2 (0%, 30%).

The conditional stability constants (β') of the copper(II) complexes were calculated at pH 5.90 based on the spectral changes via the displacement reaction with EDTA in the presence 50 mM MES and 0.1 M KCl (using 1-2 h incubation). Data for pK_a of EDTA and its Cu(II) complex taken from (8) and $\log \beta_{5.90} = 13.89$ was calculated for $[\text{Cu}(\text{EDTA})]^{2-}$. In the competition experiments the samples contained 25 μM copper(II), 25 μM ligand and the concentration of EDTA was varied in the range from 0 to 400 μM . It should be noted that EDTA and its copper(II) complex have negligible contribution to the measured absorbance values in the monitored wavelength range (320-550 nm), only $[\text{CuL}]^+$ and HL absorb light. In the case of DpC and Triapine the completion reaction was performed in 30% (w/w) DMSO/ H_2O solvent mixture. The conditional stability constants of the metal complexes (β' (CuL)) and the individual spectra of the species were calculated by the computer program PSEQUAD (31). The overall stability constants of the $[\text{CuL}]^+$ complexes (β) were calculated from the conditional stability constants: $\beta [\text{CuL}]^+ = \beta' [\text{CuL}]^+ \times \alpha_H$, where $\alpha_H = 1 + [\text{H}^+]/K_a(\text{HL}) + [\text{H}^+]^2 / (K_a(\text{HL}) \times K_a(\text{H}_2\text{L}^+))$; $[\text{H}^+] = 10^{-5.90}$ M. The overall stability constants of the protonated $[\text{CuLH}]^{2+}$ and the mixed hydroxido $[\text{CuL}(\text{OH})]$ complexes were calculated as follows: $\log \beta [\text{CuLH}]^{2+} = \log \beta [\text{CuL}]^+ + pK_a [\text{CuLH}]^{2+}$. $\log \beta [\text{CuL}(\text{OH})] = \log \beta [\text{CuL}]^+ - pK_a [\text{CuL}]^+$. $p\text{Cu} = -\log [\text{Cu}(\text{II})]$ values were calculated at pH 7.4 using the determined stability constants.

Spectrophotometric kinetic measurements

The redox reaction of the copper(II) complexes with GSH and AA was studied at 25.0 ± 0.1 °C on Hewlett Packard 8452A diode array spectrophotometer using a special, tightly closed tandem cuvette (Hellma Tandem Cell, 238-QS). The reactants were separated until the reaction was triggered. Both isolated pockets of the cuvette were completely deoxygenated by bubbling a stream of argon for 10 min before mixing the reactants. Spectra were recorded before and then immediately after the mixing, and changes were followed till no further absorbance change was observed. One of the isolated pockets contained the reducing agent (GSH or AA) and its concentration was in the range of 250-2500 μM and the other contained the copper(II) complex, which was prepared *in situ* using 25 μM of the metal ion and the ligand respectively. The pH of all the solutions was adjusted to 7.40 by 50 mM HEPES buffer and an ionic strength of 0.1 M (KCl) was applied.

The stock solutions of the reducing agents and the complexes were freshly prepared every day.

During the calculations the absorbance (A) – time (t) curves were fitted and analyzed at the λ_{\max} of the complex. $(A_0 - A_{\text{final}}) \times e^{(-a \times t)} + A_{\text{final}}$ equation was used where A_0 , A_{final} and a parameters were refined and accepted at the minimal value of the weighted sum of squared residuals (difference between the measured and calculated absorbance values) at the given wavelength. Then observed rate constants (k_{obs}) of the redox reaction were obtained from the data points of the simulated absorbance-time curves as the slope of the $\ln(A/A_0)$ versus t plots.

Cell lines and culture conditions

Human uterine sarcoma MES-SA and the doxorubicin selected MES-SA/Dx5 cells expressing mCherry and eGFP proteins, respectively, were engineered from MES-SA and MES-SA/Dx5 (ATCC; MES-SA: No. CRL-1976™, MES-SA/Dx5: No. CRL-1977™) using a lentiviral system (55). The phenotype of the resistant cells was verified using cytotoxicity assays (not shown). Prior to the experiments, MES-SA/Dx5 cells were cultured in 500 nmol/L doxorubicin, to ensure Pgp expression. Cells were cultured in DMEM (SigmaAldrich, Hungary) supplemented with 10% fetal bovine serum, 5 mmol/L glutamine, and 50 units/ml penicillin and streptomycin (Life Technologies). Human colorectal adenocarcinoma SW480 cells (obtained from ATCC; No. CCL-228™) were cultured in MEME supplemented with 10% fetal calf serum (PAA, Austria). CT-26 murine colon carcinoma cells (CRL-2638, purchased from ATCC) were cultured in Dulbecco's modified eagle's medium (DMEM)/F12 medium (1:1 from Sigma; #D6421) supplemented with 10% heat-inactivated fetal calf serum. All cell lines were cultivated at 37 °C, 5% CO₂.

Cell viability assay

In the co-culture system, after trypsinization, suspensions of MES-SA mCherry and MES-SA/Dx5 eGFP cells were mixed, and seeded on 384-well plates at a 2500 cells/well density (1250 cells/well per cell model) in 20 μ l of medium, one day prior to drug addition. Cells were then treated with a serial dilution of the drugs, so that the final volume was 60 μ l. Liquid handling was fully automated by a Hamilton StarLet robotic pipetting workstation (Hamilton, Switzerland). Plates were incubated, and measured twice: after 72 and 144 h of

drug addition. Growth inhibition of the cells was assessed based on the detection of the respective fluorescent intensities scanned from the wells by an EnSpire plate reader (eGFP: 485ex/510em; mCherry: 585ex/610em, Perkin Elmer, UK). Raw measurement files were exported, and automated data evaluation was performed by our custom program, which was written by Judit Sessler in C#. Data was normalized to the negative (live cells, maximal fluorescence) and positive (dead cells, minimal fluorescence) controls, then growth inhibition data points (plotted against the respective concentrations) were connected with a line, and IC_{50} was considered as the point, at which the connecting line reached the 50% inhibition according to the Y axis.

For single cell viability assay, SW480 cells were plated (2×10^3 cells/well) in 96-well plates and allowed to recover for 24 h. Then, cells were treated with increasing concentrations of TSCs for 72 h. Cell viability was measured by the 3-(4,5-dimethylthiazol-2-yl)-2,5-diphenyltetrazolium bromide (MTT)-based vitality assay (EZ4U; Biomedica, Vienna, Austria) as published (17). GraphPad Prism software was used to calculate cell viability expressed as IC_{50} values calculated from full dose-response curves. For further analysis and comparison, pIC_{50} values were used instead of IC_{50} values (Suppl. Figure 1). pIC_{50} values were calculated as the $-\log_{10}$ from IC_{50} values in molar.

Microscopy

Cells were seeded into a 24-well plate with 2×10^4 cells/well and left to recover for 24 h. Then, cells were treated with indicated concentrations of TSC ligands. After 24 or 48 h, microscopic phase-contrast images were taken with a Zeiss primo vert microscope with a Zeiss axio cam ERC5s camera. Percentage of vacuolated cells was counted in at least three different parts of a well.

Quantification of superoxide radicals

To examine the cell-free production of superoxide radicals, the reduction of NBT was analyzed as previously reported (27). Briefly, 0.6 mM NBT was incubated with 5 μ M copper(II) complexes with or without 2 mM NAC. The experiments were performed in PBS (pH 7.4). The extent of NBT reduction was determined spectrophotometrically by measuring the absorbance at 560 nm after 45 min of incubation. No superoxide radicals were observed without NAC (data not shown).

Intracellular superoxide determination using DHE

DHE (#D7008, Sigma-Aldrich, MO, USA) was used to detect the production of intracellular superoxide. Briefly, 5×10^5 MES-SA cells per sample in 500 μ l of PBS (78.1 mM $\text{Na}_2\text{PO}_4 \times 2 \text{H}_2\text{O}$, 14.7 mM KH_2PO_4 , 26.8 mM KCl, 1.37 M NaCl) were incubated with or without 2 mM NAC for 15 min at 37°C. Then, 5 μ M of indicated TSC complexes were added for further 60 min. Subsequently, DHE (10 μ M) was added 30 min before measurement. After incubation, the mean fluorescence intensity was measured by flow cytometry using a FACSCalibur instrument (Becton Dickinson, Palo Alto, CA, USA). Antimycin A (AMA, 10 μ M) was used as positive control.

PDI reduction activity measurement

PDI reduction activity was measured using PROTEOSTAT PDI assay kit (#ENZ-51024, Enzo Life Sciences, Switzerland). Experiments were performed according to the manufacturer's instructions. Briefly, drugs alone or preincubated with CuCl_2 (1:1) were added to a prepared insulin PDI solution. Then, dithiothreitol (DTT) (1 mM) was added to start PDI reduction activity. After 30 min the reaction was stopped by the Stop reagent and the insulin precipitate was fluorescently labeled with Proteostat PDI detection reagent for 15 min. Fluorescence intensity was measured at 500 nm excitation and 603 nm emission using the spectrophotometer Tecan infinite 200Pro (Tecan Group, Männedorf, Switzerland).

Protein expression

After drug treatment, total protein lysates were prepared, 20 μ g per sample separated by SDS-PAGE and transferred onto a polyvinylidene difluoride membrane for Western blotting as described previously (17). The following antibodies were used: Cell Signaling Technology (MA, USA): SOD2 (#13141), GAPDH (#5174). Primary antibodies were used 1:1000. Secondary anti-rabbit (#7074) horseradish peroxidase-labeled antibodies from Cell Signaling Technologies were used in working dilutions of 1:10 000.

Total-RNA isolation and whole genome gene expression array

Total RNA from SW480 cells (either untreated or treated (0.1 or 1 μ M for 15 h)) was isolated using RNeasy Mini kit (#74106, Quiagen, Germany) following the manufacturer's instruction. Transcriptional profiles of cells were determined performing a 4 \times 44K whole genome oligonucleotide gene expression array (Agilent, California, US) as described

previously (32). Normalization was performed in R using the Bioconductor (version 3.7) package “limma” if not otherwise indicated (42). Whole genome gene expression array and gene set enrichment analysis (GSEA) were performed as previously described (13).

Animal experiments

Six- to eight-week-old BALB/c mice were purchased from Janvier (France). The animals were kept in a pathogen-free environment and every procedure was done in a laminar airflow cabinet. Experiments were done according to the regulations of the Ethics Committee for the Care and Use of Laboratory Animals at the Medical University Vienna (proposal number BMWF-66.009/0081-WF/V/3b/2015), the U.S. Public Health Service Policy on Human Care and Use of Laboratory Animals as well as the United Kingdom Coordinating Committee on Cancer Prevention Research's Guidelines for the Welfare of Animals in Experimental Neoplasia. To ensure animal welfare throughout the experiment, the body weight of the mice was assessed once a day. At weight loss exceeding 10 % (in less than two days) or occurrence of ascites, animals were sacrificed by cervical dislocation.

***In vivo* analysis of SOD2 expression**

CT-26 cells (5×10^5 cells in 50 μ l) were injected subcutaneously into the right flank of female Balb/c mice. Starting on day 4, Triapine (10 mg/kg in 10% DMSO) or solvent treatment was given orally for 5 consecutive days a week for two weeks. Animals were sacrificed on indicated days per cervical dislocation and tumor tissue was isolated and fixed in 4% paraformaldehyde (Carl Roth, #P087.3) for 24 h. Tumor tissue was paraffin-embedded with the KOS machine (Milestone) and sliced in 4 μ m thick sections. For SOD2 staining, sections were incubated with a SOD2-specific antibody (1:1000, Cell Signaling, #13141) in a humid chamber for 1 h at room temperature after antigen retrieval by boiling for 30 min in 10 mM citrate buffer (pH 6.0, DAKO; #S1699),. Antibody binding was detected using the UltraVision LP detection system according to the manufacturer's instructions (Thermo Fisher Scientific Inc.; #TL-125-HL). Color was developed using 3,3'-diaminobenzidine (Dako; #K3468), followed by a nuclear counterstain with hematoxylin. Stained tissue slides were scanned and analyzed using Definiens Software.

Correlation analysis

Correlations were performed in the GraphPad Prism 8 software. R_2 from linear or one phase decay regression are given in correlation diagrams. Regressions lines are shown in correlation plots with 95% confidence interval. P-values were calculated using Pearson correlation coefficient which is a measure of linear correlation. For the correlation matrix (Figure 6D) p-values of correlations were corrected for multiple comparisons with two-stage linear step-up procedure of Benjamini, Krieger and Yekutieli with a false discovery rate (FDR) of 1%. The thereby generated q-values are shown with a greyscale code.

Acknowledgments

This work was supported by the National Research, Development and Innovation Office-NKFI through project FK 124240 and FIKP program TUDFO/47138-1/2019-ITM. Furthermore, this work was in part funded by the Austrian Science Fund (FWF) grant number P31923 (to C.R. Kowol and P. Heffeter). S. Hager is a recipient of a DOC Fellowship of the Austrian Academy of Sciences. The funding sources had no involvement in collection, analysis and interpretation of data as well as in the decision to submit the article for publication.

Author Disclosure Statement:

The authors declare no conflict of interest.

List of Abbreviations

- AA – ascorbic acid
- AMA – antimycin A
- dd – double distilled
- DHE - dihydroethidium
- DMSO – dimethyl sulfoxide
- Dp44mT - di-2-pyridylketone 4,4-dimethyl-3-thiosemicarbazone
- DpC – di-2-pyridylketone 4-cyclohexyl-4-methyl-3-thiosemicarbazone
- DTT – dithiothreitol
- EDTA – ethylenediaminetetraacetic acid
- ER – endoplasmic reticulum
- FDR – false discovery rate
- FTSC - 2-formylpyridine thiosemicarbazone
- GSEA – gene set enrichment analysis
- GSH – glutathione
- HEPES - 4-(2-hydroxyethyl)-1-piperazineethanesulfonic acid
- MDR – multidrug resistant
- MES - 2-(*N*-morpholino)ethanesulfonic acid
- MT – metallothionein
- MTT - 3-(4,5-dimethylthiazol-2-yl)-2,5-diphenyltetrazolium bromide
- NAC – *N*-acetyl cysteine
- NBT- nitroblue tetrazolium
- PDI – protein disulfide isomerase
- P-gp – P-glycoprotein (ABCB1)
- PTSC - pyridine-2-carbaldehyde thiosemicarbazone
- RR – ribonucleotide reductase
- ROS – reactive oxygen species
- SOD – superoxide dismutase
- TSC – thiosemicarbazone
- UV-vis – UV-visible

References

1. Antholine W, Knight J, Whelan H, Petering DH. Studies of the reaction of 2-formylpyridine thiosemicarbazone and its iron and copper complexes with biological systems. *Mol Pharmacol* 13: 89-98, 1977.
2. Bacher F, Domotor O, Kaltenbrunner M, Mojovic M, Popovic-Bijelic A, Graslund A, Ozarowski A, Filipovic L, Radulovic S, Enyedy EA, Arion VB. Effects of terminal dimethylation and metal coordination of proline-2-formylpyridine thiosemicarbazone hybrids on lipophilicity, antiproliferative activity, and hR2 RNR inhibition. *Inorg Chem* 53: 12595-609, 2014.
3. Brady DC, Crowe MS, Turski ML, Hobbs GA, Yao X, Chaikuad A, Knapp S, Xiao K, Campbell SL, Thiele DJ, Counter CM. Copper is required for oncogenic BRAF signalling and tumorigenesis. *Nature* 509: 492-6, 2014.
4. Covington AK, Dickinson T. *Physical chemistry of organic solvent systems* London, New York,: Plenum Press; 1973. x, 823 p. p.
5. Domotor O, May NV, Pelivan K, Kiss T, Keppler BK, Kowol CR, Enyedy EA. A comparative study of alpha-N-pyridyl thiosemicarbazones: Spectroscopic properties, solution stability and copper(II) complexation. *Inorg Chim Acta* 472: 264-275, 2018.
6. Enyedy EA, Nagy NV, Zsigo E, Kowol CR, Arion VB, Keppler BK, Kiss T. Comparative Solution Equilibrium Study of the Interactions of Copper(II), Iron(II) and Zinc(II) with Triapine (3-Aminopyridine-2-carbaldehyde Thiosemicarbazone) and Related Ligands. *Eur J Inorg Chem*: 1717-1728, 2010.
7. Enyedy EA, Primik MF, Kowol CR, Arion VB, Kiss T, Keppler BK. Interaction of Triapine and related thiosemicarbazones with iron(III)/(II) and gallium(III): a comparative solution equilibrium study. *Dalton Trans* 40: 5895-5905, 2011.
8. Felcman J, da Silva JJ. Complexes of oxovanadium(IV) with polyaminocarboxylic acids. *Talanta* 30: 565-70, 1983.

9. Furedi A, Toth S, Szebenyi K, Pape VF, Turk D, Kucsma N, Cervenak L, Tovari J, Szakacs G. Identification and Validation of Compounds Selectively Killing Resistant Cancer: Delineating Cell Line-Specific Effects from P-Glycoprotein-Induced Toxicity. *Mol Cancer Ther* 16: 45-56, 2017.
10. Gaetke LM, Chow-Johnson HS, Chow CK. Copper: toxicological relevance and mechanisms. *Arch Toxicol* 88: 1929-1938, 2014.
11. Garcia-Tojal J, Gil-Garcia R, Fouz VI, Madariaga G, Lezama L, Galletero MS, Borrás J, Nollmann FI, Garcia-Giron C, Alcaraz R, Cavia-Saiz M, Muniz P, Palacios O, Samper KG, Rojo T. Revisiting the thiosemicarbazonecopper(II) reaction with glutathione. Activity against colorectal carcinoma cell lines. *J Inorg Biochem* 180: 69-79, 2018.
12. Giles FJ, Fracasso PM, Kantarjian HM, Cortes JE, Brown RA, Verstovsek S, Alvarado Y, Thomas DA, Faderl S, Garcia-Manero G, Wright LP, Samson T, Cahill A, Lambert P, Plunkett W, Sznol M, DiPersio JF, Gandhi V. Phase I and pharmacodynamic study of Triapine, a novel ribonucleotide reductase inhibitor, in patients with advanced leukemia. *Leuk Res* 27: 1077-83, 2003.
13. Hager S, Korbula K, Bielec B, Grusch M, Pirker C, Schosserer M, Liendl L, Lang M, Grillari J, Nowikovsky K, Pape VFS, Mohr T, Szakacs G, Keppler BK, Berger W, Kowol CR, Heffeter P. The thiosemicarbazone Me₂NNMe₂ induces paraptosis by disrupting the ER thiol redox homeostasis based on protein disulfide isomerase inhibition. *Cell Death Dis* 9: 1052, 2018.
14. Hancock CN, Stockwin LH, Han B, Divelbiss RD, Jun JH, Malhotra SV, Hollingshead MG, Newton DL. A copper chelate of thiosemicarbazone NSC 689534 induces oxidative/ER stress and inhibits tumor growth in vitro and in vivo. *Free Radic Biol Med* 50: 110-21, 2011.
15. Hartinger CG, Zorbas-Seifried S, Jakupec MA, Kynast B, Zorbas H, Keppler BK. From bench to bedside - preclinical and early clinical development of the anticancer agent indazolium trans-[tetrachlorobis(1H-indazole)ruthenate(III)] (KP1019 or FFC14A). *J Inorg Biochem* 100: 891-904, 2006.
16. Heffeter P, Pape VFS, Enyedy EA, Keppler BK, Szakacs G, Kowol CR. Anticancer Thiosemicarbazones: Chemical Properties, Interaction with Iron Metabolism, and Resistance Development. *Antioxid Redox Signal* 30: 1062-1082, 2019.

This paper has been peer-reviewed and accepted for publication, but has yet to undergo copyediting and proof correction. The final published version may differ from this proof.

High copper complex stability and slow reduction kinetics as key parameters for improved activity, paraptosis induction and impact on drug-resistant cells of anticancer thiosemicarbazones (DOI: 10.1089/ars.2019.7854)

Antioxidants and Redox Signaling

Downloaded by Northwestern University from www.liebertpub.com at 05/03/20. For personal use only.

17. Heffeter P, Pongratz M, Steiner E, Chiba P, Jakupec MA, Elbling L, Marian B, Korner W, Sevelda F, Micksche M, Keppler BK, Berger W. Intrinsic and acquired forms of resistance against the anticancer ruthenium compound KP1019 [indazolium trans-[tetrachlorobis(1H-indazole)ruthenate (III)] (FFC14A)]. *J Pharmacol Exp Ther* 312: 281-9, 2005.
18. Irving HM, Miles MG, Pettit LD. A Study of Some Problems in Determining Stoichiometric Proton Dissociation Constants of Complexes by Potentiometric Titrations Using a Glass Electrode. *Anal Chim Acta* 38: 475-+, 1967.
19. Ishiguro K, Lin ZP, Penketh PG, Shyam K, Zhu R, Baumann RP, Zhu YL, Sartorelli AC, Rutherford TJ, Ratner ES. Distinct mechanisms of cell-kill by triapine and its terminally dimethylated derivative Dp44mT due to a loss or gain of activity of their copper(II) complexes. *Biochem Pharmacol* 91: 312-22, 2014.
20. Jansson PJ, Sharpe PC, Bernhardt PV, Richardson DR. Novel thiosemicarbazones of the ApT and DpT series and their copper complexes: identification of pronounced redox activity and characterization of their antitumor activity. *J Med Chem* 53: 5759-69, 2010.
21. Jansson PJ, Yamagishi T, Arvind A, Seebacher N, Gutierrez E, Stacy A, Maleki S, Sharp D, Sahni S, Richardson DR. Di-2-pyridylketone 4,4-dimethyl-3-thiosemicarbazone (Dp44mT) overcomes multidrug resistance by a novel mechanism involving the hijacking of lysosomal P-glycoprotein (Pgp). *J Biol Chem* 290: 9588-603, 2015.
22. Jungwirth U, Kowol CR, Keppler BK, Hartinger CG, Berger W, Heffeter P. Anticancer activity of metal complexes: involvement of redox processes. *Antioxid Redox Signal* 15: 1085-127, 2011.
23. Kalinowski DS, Stefani C, Toyokuni S, Ganz T, Anderson GJ, Subramaniam NV, Trinder D, Olynyk JK, Chua A, Jansson PJ, Sahni S, Lane DJ, Merlot AM, Kovacevic Z, Huang ML, Lee CS, Richardson DR. Redox cycling metals: Pedaling their roles in metabolism and their use in the development of novel therapeutics. *Biochim Biophys Acta* 1863: 727-48, 2016.

24. Kallus S, Uhlik L, van Schoonhoven S, Pelivan K, Berger W, Enyedy EA, Hofmann T, Heffeter P, Kowol CR, Keppler BK. Synthesis and biological evaluation of biotin-conjugated anticancer thiosemicarbazones and their iron(III) and copper(II) complexes. *J Inorg Biochem* 190: 85-97, 2019.
25. Karp JE, Giles FJ, Gojo I, Morris L, Greer J, Johnson B, Thein M, Sznol M, Low J. A phase I study of the novel ribonucleotide reductase inhibitor 3-aminopyridine-2-carboxaldehyde thiosemicarbazone (3-AP, Triapine) in combination with the nucleoside analog fludarabine for patients with refractory acute leukemias and aggressive myeloproliferative disorders. *Leuk Res* 32: 71-7, 2008.
26. Kontoghiorghes GJ, Efstathiou A, Loannou-Loucaides S, Kolnagou A. Chelators controlling metal metabolism and toxicity pathways: Applications in cancer prevention, diagnosis and treatment. *Hemoglobin* 32: 217-227, 2008.
27. Kowol CR, Heffeter P, Miklos W, Gille L, Trondl R, Cappellacci L, Berger W, Keppler BK. Mechanisms underlying reductant-induced reactive oxygen species formation by anticancer copper(II) compounds. *J Biol Inorg Chem* 17: 409-23, 2012.
28. Kowol CR, Miklos W, Pfaff S, Hager S, Kallus S, Pelivan K, Kubanik M, Enyedy EA, Berger W, Heffeter P, Keppler BK. Impact of Stepwise NH₂-Methylation of Triapine on the Physicochemical Properties, Anticancer Activity, and Resistance Circumvention. *J Med Chem* 59: 6739-52, 2016.
29. Kowol CR, Trondl R, Heffeter P, Arion VB, Jakupec MA, Roller A, Galanski M, Berger W, Keppler BK. Impact of metal coordination on cytotoxicity of 3-aminopyridine-2-carboxaldehyde thiosemicarbazone (triapine) and novel insights into terminal dimethylation. *J Med Chem* 52: 5032-43, 2009.
30. Kunos CA, Ivy SP. Triapine Radiochemotherapy in Advanced Stage Cervical Cancer. *Front Oncol* 8: 149, 2018.
31. L. Zékány IN. Computational Methods for the Determination of Stability Constants. In: *Computational Methods for the Determination of Stability Constants*. edited by Leggett DJ. New York: Springer US; 1985. pp. 291-353.

This paper has been peer-reviewed and accepted for publication, but has yet to undergo copyediting and proof correction. The final published version may differ from this proof.

High copper complex stability and slow reduction kinetics as key parameters for improved activity, paraptosis induction and impact on drug-resistant cells of anticancer thiosemicarbazones (DOI: 10.1089/ars.2019.7854)

Antioxidants and Redox Signaling

Downloaded by Northwestern University from www.liebertpub.com at 05/03/20. For personal use only.

32. Laszlo V, Hoda MA, Garay T, Pirker C, Ghanim B, Klikovits T, Dong YW, Rozsas A, Kenessey I, Szirtes I, Grusch M, Jakopovic M, Samarzija M, Brcic L, Kern I, Rozman A, Popper H, Zochbauer-Muller S, Heller G, Altenberger C, Ziegler B, Klepetko W, Berger W, Dome B, Hegedus B. Epigenetic down-regulation of integrin alpha7 increases migratory potential and confers poor prognosis in malignant pleural mesothelioma. *J Pathol* 237: 203-14, 2015.
33. Lee D, Kim IY, Saha S, Choi KS. Paraptosis in the anti-cancer arsenal of natural products. *Pharmacol Ther* 162: 120-33, 2016.
34. Lovejoy DB, Jansson PJ, Brunk UT, Wong J, Ponka P, Richardson DR. Antitumor activity of metal-chelating compound Dp44mT is mediated by formation of a redox-active copper complex that accumulates in lysosomes. *Cancer Res* 71: 5871-80, 2011.
35. Lovejoy DB, Sharp DM, Seebacher N, Obeidy P, Prichard T, Stefani C, Basha MT, Sharpe PC, Jansson PJ, Kalinowski DS, Bernhardt PV, Richardson DR. Novel second-generation di-2-pyridylketone thiosemicarbazones show synergism with standard chemotherapeutics and demonstrate potent activity against lung cancer xenografts after oral and intravenous administration in vivo. *J Med Chem* 55: 7230-44, 2012.
36. Malarz K, Mrozek-Wilczkiewicz A, Serda M, Rejmund M, Polanski J, Musiol R. The role of oxidative stress in activity of anticancer thiosemicarbazones. *Oncotarget* 9: 17689-17710, 2018.
37. Maleki Vareki S, Salim KY, Danter WR, Koropatnick J. Novel anti-cancer drug COTI-2 synergizes with therapeutic agents and does not induce resistance or exhibit cross-resistance in human cancer cell lines. *PLoS One* 13: e0191766, 2018.
38. McGivern TJP, Afsharpour S, Marmion CJ. Copper complexes as artificial DNA metallonucleases: From Sigman's reagent to next generation anti-cancer agent? *Inorg Chim Acta* 472: 12-39, 2018.
39. Merlot AM, Porter GM, Sahni S, Lim EG, Peres P, Richardson DR. The metastasis suppressor, NDRG1, differentially modulates the endoplasmic reticulum stress response. *Biochim Biophys Acta Mol Basis Dis* 1865: 2094-2110, 2019.

40. Pape VF, Toth S, Furedi A, Szebenyi K, Lovrics A, Szabo P, Wiese M, Szakacs G. Design, synthesis and biological evaluation of thiosemicarbazones, hydrazinobenzothiazoles and arylhydrazones as anticancer agents with a potential to overcome multidrug resistance. *Eur J Med Chem* 117: 335-54, 2016.
41. Pham AN, Xing GW, Miller CJ, Waite TD. Fenton-like copper redox chemistry revisited: Hydrogen peroxide and superoxide mediation of copper-catalyzed oxidant production. *Journal of Catalysis* 301: 54-64, 2013.
42. Ritchie ME, Phipson B, Wu D, Hu Y, Law CW, Shi W, Smyth GK. limma powers differential expression analyses for RNA-sequencing and microarray studies. *Nucleic Acids Res* 43: e47, 2015.
43. Ruttkay-Nedecky B, Nejdil L, Gumulec J, Zitka O, Masarik M, Eckschlager T, Stiborova M, Adam V, Kizek R. The role of metallothionein in oxidative stress. *Int J Mol Sci* 14: 6044-66, 2013.
44. Santoro A, Vileno B, Palacios O, Peris-Diaz MD, Riegel G, Gaiddon C, Krezel A, Faller P. Reactivity of Cu(ii)-, Zn(ii)- and Fe(ii)-thiosemicarbazone complexes with glutathione and metallothionein: from stability to dissociation to transmetallation. *Metallomics* 11: 994-1004, 2019.
45. Schafer FQ, Buettner GR. Redox environment of the cell as viewed through the redox state of the glutathione disulfide/glutathione couple. *Free Radical Bio Med* 30: 1191-1212, 2001.
46. Seebacher NA, Richardson DR, Jansson PJ. A mechanism for overcoming P-glycoprotein-mediated drug resistance: novel combination therapy that releases stored doxorubicin from lysosomes via lysosomal permeabilization using Dp44mT or DpC. *Cell Death Dis* 7: e2510, 2016.
47. Serda M, Kalinowski DS, Rasko N, Potuckova E, Mrozek-Wilczkiewicz A, Musiol R, Malecki JG, Sajewicz M, Ratuszna A, Muchowicz A, Golab J, Simunek T, Richardson DR, Polanski J. Exploring the anti-cancer activity of novel thiosemicarbazones generated through the combination of retro-fragments: dissection of critical structure-activity relationships. *PLoS One* 9: e110291, 2014.

This paper has been peer-reviewed and accepted for publication, but has yet to undergo copyediting and proof correction. The final published version may differ from this proof.

High copper complex stability and slow reduction kinetics as key parameters for improved activity, paraptosis induction and impact on drug-resistant cells of anticancer thiosemicarbazones (DOI: 10.1089/ars.2019.7854)

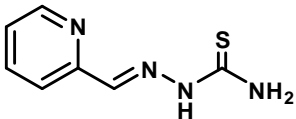
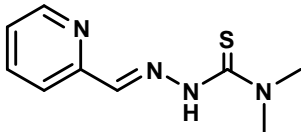
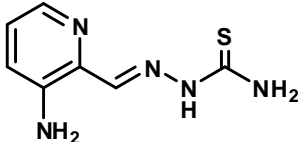
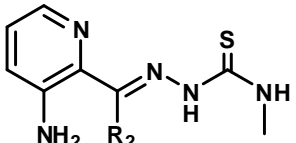
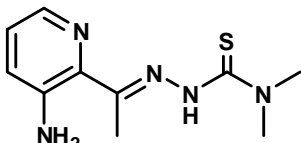
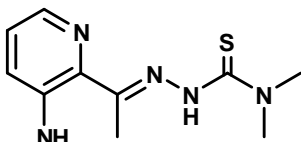
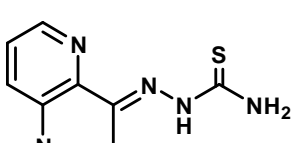
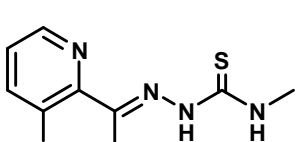
Antioxidants and Redox Signaling

Downloaded by Northwestern University from www.liebertpub.com at 05/03/20. For personal use only.

48. Shao J, Zhou B, Di Bilio AJ, Zhu L, Wang T, Qi C, Shih J, Yen Y. A Ferrous-Triapine complex mediates formation of reactive oxygen species that inactivate human ribonucleotide reductase. *Mol Cancer Ther* 5: 586-92, 2006.
49. Shimada K, Reznik E, Stokes ME, Krishnamoorthy L, Bos PH, Song Y, Quartararo CE, Pagano NC, Carpizo DR, deCarvalho AC, Lo DC, Stockwell BR. Copper-Binding Small Molecule Induces Oxidative Stress and Cell-Cycle Arrest in Glioblastoma-Patient-Derived Cells. *Cell Chem Biol* 25: 585-594 e7, 2018.
50. Sperandio S, de Belle I, Bredesen DE. An alternative, nonapoptotic form of programmed cell death. *Proc Natl Acad Sci U S A* 97: 14376-81, 2000.
51. Srivastava S, Blower PJ, Aubdool AA, Hider RC, Mann GE, Siow RC. Cardioprotective effects of Cu(II)ATSM in human vascular smooth muscle cells and cardiomyocytes mediated by Nrf2 and DJ-1. *Sci Rep* 6: 7, 2016.
52. Stacy AE, Palanimuthu D, Bernhardt PV, Kalinowski DS, Jansson PJ, Richardson DR. Structure-Activity Relationships of Di-2-pyridylketone, 2-Benzoylpyridine, and 2-Acetylpyridine Thiosemicarbazones for Overcoming Pgp-Mediated Drug Resistance. *J Med Chem* 59: 8601-20, 2016.
53. Trondl R, Flocke LS, Kowol CR, Heffeter P, Jungwirth U, Mair GE, Steinborn R, Enyedy EA, Jakupec MA, Berger W, Keppler BK. Triapine and a more potent dimethyl derivative induce endoplasmic reticulum stress in cancer cells. *Mol Pharmacol* 85: 451-9, 2014.
54. Turk D, Hall MD, Chu BF, Ludwig JA, Fales HM, Gottesman MM, Szakacs G. Identification of compounds selectively killing multidrug-resistant cancer cells. *Cancer Res* 69: 8293-301, 2009.
55. Windt T, Toth S, Patik I, Sessler J, Kucsma N, Szepesi A, Zdrzil B, Ozvegy-Laczka C, Szakacs G. Identification of anticancer OATP2B1 substrates by an in vitro triple-fluorescence-based cytotoxicity screen. *Arch Toxicol* 93: 953-964, 2019.
56. Yee KW, Cortes J, Ferrajoli A, Garcia-Manero G, Verstovsek S, Wierda W, Thomas D, Faderl S, King I, O'Brien S M, Jeha S, Andreeff M, Cahill A, Sznol M, Giles FJ. Triapine and cytarabine is an active combination in patients with acute leukemia or myelodysplastic syndrome. *Leuk Res* 30: 813-22, 2006.

57. Yu Y, Gutierrez E, Kovacevic Z, Saletta F, Obeidy P, Suryo Rahmanto Y, Richardson DR. Iron chelators for the treatment of cancer. *Curr Med Chem* 19: 2689-702, 2012.
58. Yu Y, Suryo Rahmanto Y, Hawkins CL, Richardson DR. The potent and novel thiosemicarbazone chelators di-2-pyridylketone-4,4-dimethyl-3-thiosemicarbazone and 2-benzoylpyridine-4,4-dimethyl-3-thiosemicarbazone affect crucial thiol systems required for ribonucleotide reductase activity. *Mol Pharmacol* 79: 921-31, 2011.
59. Zeidner JF, Karp JE, Blackford AL, Smith BD, Gojo I, Gore SD, Levis MJ, Carraway HE, Greer JM, Ivy SP, Pratz KW, McDevitt MA. A phase II trial of sequential ribonucleotide reductase inhibition in aggressive myeloproliferative neoplasms. *Haematologica* 99: 672-8, 2014.
60. Zhang C. Essential functions of iron-requiring proteins in DNA replication, repair and cell cycle control. *Protein Cell* 5: 750-60, 2014.

Table 1: Structure and IC₅₀ (72 h) values of tested compounds in SW480 cells.

Compound	Structure	TSC IC ₅₀ (μM)	Cu-TSC IC ₅₀ (μM)
FTSC		6.54 ± 0.22	6.01 ± 0.54
PTSC		0.051 ± 0.025	0.057 ± 0.024
Triapine		0.68 ± 0.18	1.19 ± 0.61
H ₂ NNHMe		2.54 ± 0.61	3.13 ± 1.48
H ₂ NNMe ₂		0.80 ± 0.12	1.62 ± 0.28
MeHNNMe ₂		2.28 ± 0.17	3.30 ± 0.83
Me ₂ NNH ₂		8.51 ± 1.18	4.97 ± 1.57
Me ₂ NNHMe		7.80 ± 2.06	0.93 ± 0.38

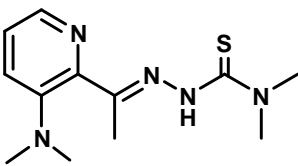
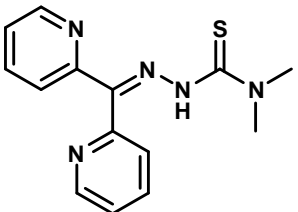
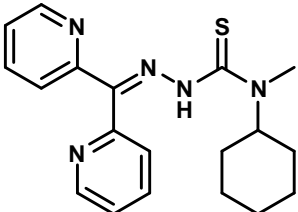
Me ₂ NNMe ₂		0.038 ± 0.012	0.066 ± 0.020
Dp44mT		0.047 ± 0.018	0.034 ± 0.013
DpC		0.043 ± 0.017	0.039 ± 0.012

Table 2: IC₅₀ (72 h) values of tested compounds in MES-SA and MES-SA/Dx5 cells.

	TSC IC ₅₀ (μM)		Cu-TSC IC ₅₀ (μM)	
	MES-SA	MES-SA/Dx5 (resistance factor)	MES-SA	MES-SA/Dx5 (resistance factor)
FTSC	1.87 ± 0.22	8.11 ± 0.94 (4.3)	9.45 ± 0.49	4.31 ± 0.72 (0.46)
PTSC	0.129 ± 0.032	0.029 ± 0.003 (0.22)	0.081 ± 0.046	0.024 ± 0.005 (0.30)
Triapine	0.63 ± 0.09	2.58 ± 0.33 (4.1)	2.44 ± 0.47	16.86 ± 2.15 (6.9)
H ₂ NNHMe	0.86 ± 0.10	4.05 ± 0.39 (4.7)	6.75 ± 1.31	21.35 ± 3.35 (3.2)
H ₂ NNMe ₂	0.51 ± 0.13	0.76 ± 0.17 (1.5)	2.57 ± 0.47	4.19 ± 0.24 (1.6)
MeHNNMe ₂	0.99 ± 0.12	2.76 ± 0.00 (2.8)	6.22 ± 1.43	2.13 ± 0.47 (0.34)
Me ₂ NNH ₂	3.51 ± 0.55	3.29 ± 0.74 (0.94)	9.91 ± 1.22	3.24 ± 0.29 (0.33)
Me ₂ NNHMe	2.57 ± 0.31	2.24 ± 0.51 (0.87)	3.58 ± 0.97	1.13 ± 0.13 (0.32)
Me ₂ NNMe ₂	0.013 ± 0.002	0.004 ± 0.001 (0.31)	0.030 ± 0.018	0.008 ± 0.002 (0.27)
Dp44mT	0.029 ± 0.015	0.006 ± 0.001 (0.21)	0.066 ± 0.039	0.004 ± 0.001 (0.06)
DpC	0.034 ± 0.027	0.003 ± 0.002 (0.09)	0.009 ± 0.007	0.001 ± 0.0008 (0.11)

Table 3: pK_a values of the TSC ligands determined by spectrophotometric titrations and overall stability constants for the copper(II) TSC complexes ($\log\beta$)^{*} calculated from the conditional stability constants ($\log\beta'_{5.9}$ of $[\text{CuL}]^+$) and pK_a values of the copper(II) complexes. $p\text{Cu} = -\log [\text{Cu(II)}]$ values calculated at pH 7.4 $c_{\text{Cu(II)}} = c_{\text{TSC}} = 1 \mu\text{M}$ and fraction of $[\text{CuL(OH)}]$.

ligand	mediu m	pK_a (H_2L^+)	pK_a (HL)	$\log\beta$ $[\text{CuLH}]^2$ +	$\log\beta$ [CuL] +	$\log\beta$ [CuL(OH)]	pCu	% [CuL(OH)]
FTSC	H ₂ O	3.48 ± 0.01	10.72±0.0	20.34	18.26	9.56	11.9 6	4.8
PTSC	H ₂ O	3.61 ± 0.01	10.22±0.0	21.05	18.96	10.40	13.1 7	6.5
Triapine [*]	H ₂ O	4.25	10.58	20.08	17.57	8.93	11.3 5	5.4
H ₂ NNHMe	H ₂ O	4.40 ± 0.01	11.03±0.0	20.26	17.72	9.10	11.1 2	5.7
H ₂ NNMe ₂	H ₂ O	4.64 ± 0.01	10.09±0.0	20.84	18.33	9.68	12.6 6	5.3
MeHNNMe ₂	H ₂ O	4.87 ± 0.01	9.87±0.01	20.80	18.16	9.97	12.7 5	14.0
Me ₂ NNH ₂	H ₂ O	4.43	10.87±0.0	20.56	18.25	9.72	11.8	6.9

			±	1				1	
			0.01						
Me ₂ NNHM	H ₂ O	4.53	10.98±0.0	21.02	18.45	10.34	11.9	16.3	
e		±	7				5		
		0.02							
Me ₂ NNMe ₂	H ₂ O	4.93	10.69±0.0	22.06	19.55	10.77	13.2	4.0	
		±	1				8		
		0.01							
Dp44mT	H ₂ O	3.44	10.44±0.0	21.77	19.43	10.64	13.4	3.9	
		±	1				1		
		0.01							
DpC	5%	3.47	10.71±0.0	-	-	-	-	-	
	DMSO	±	1						
		0.01							
DpC	30%	3.03	11.38±0.0	19.28	17.15	7.69	10.1	0.9	
	DMSO	±	6				7		
		0.06							
DpC [†]	H ₂ O	3.50	10.67	22.81	20.36	12.00	14.1	9.9	
							3		
Triapine [‡]	30%	3.92	10.78	16.69	14.35	4.68	8.55	0.5	
	DMSO								
H ₂ NNMe ₂ [‡]	30%	4.31	10.29	17.05	15.12	5.63	9.38	0.8	
	DMSO								

* pK_a taken from Ref. (20). [†] Estimated values from the pK_a values of DpC ligand measured in 5% and 30% (w/w) DMSO/H₂O mixtures. [‡] Data taken from Ref.(5).

Table 4: Calculated observed rate constants (k_{obs}) and half-lives ($t_{1/2}$) in the copper(II) – TSC – GSH (1:1:50) systems from the spectral changes at the λ_{max} of the copper(II) complex and absorbance values measured at 1 h compared to that of the ligand.

	k_{obs} (min^{-1})	$t_{1/2}$ (min)	λ (nm)	fraction of non-reduced Cu(II)-complex at 1 h (%)
FTSC	4.13×10^{-2}	17	380	10
PTSC [*]	4.30×10^{-4}	1615	394	90
Triapine [†]	1.10×10^{-1}	6	420	4
H ₂ NNHMe	7.70×10^{-2}	9	420	10
H ₂ NNMe ₂	1.60×10^{-2}	44	424	61
MeHNNMe ₂	1.12×10^{-2}	62	450	57
Me ₂ NNH ₂	4.47×10^{-2}	16	416	24
Me ₂ NNHMe	3.90×10^{-2}	18	420	20
Me ₂ NNMe ₂	6.97×10^{-4}	1019	422	92
Dp44mT	2.12×10^{-3}	329	412	80
DpC	2.30×10^{-3}	298	422	85
FTSC	4.13×10^{-2}	17	380	10
PTSC [†]	4.30×10^{-4}	1615	394	90

* $k_{\text{obs}} = 1.03 \times 10^{-3} \text{ min}^{-1}$, $t_{1/2} = 675 \text{ min}$ in the presence of 100 eq. GSH (20).[†] $k_{\text{obs}} = 6.30 \times 10^{-2} \text{ min}^{-1}$, $t_{1/2} = 11 \text{ min}$ in the presence of 20 eq. GSH; $k_{\text{obs}} = 5.90 \times 10^{-2} \text{ min}^{-1}$, $t_{1/2} = 12 \text{ min}$ in the presence of 10 eq. GSH.

Figure Legends

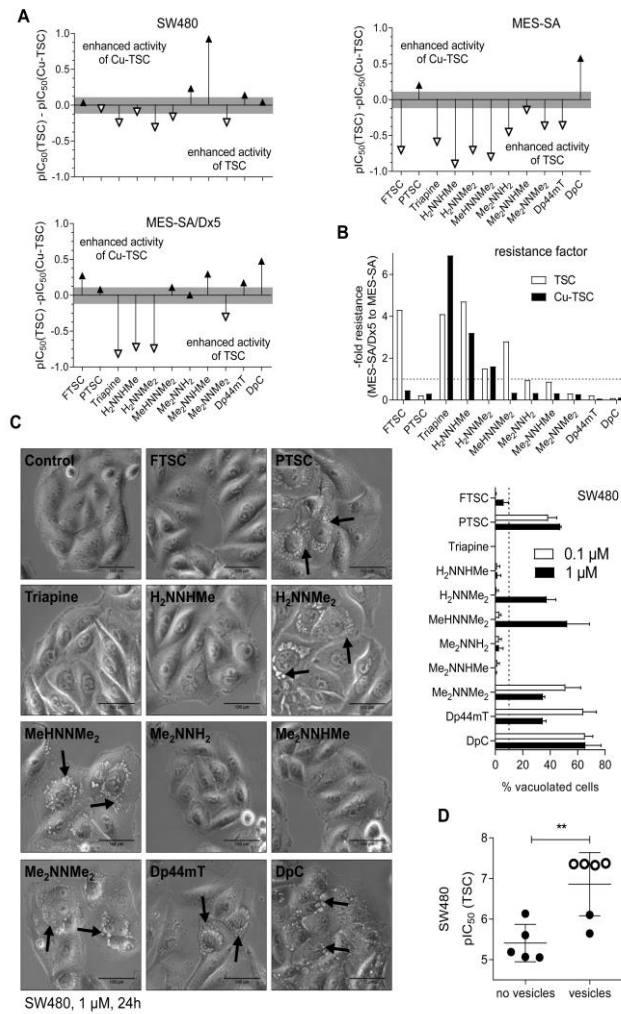


Figure 1: Change of anticancer activity upon complexation with copper(II) and potential of the tested TSC panel to induce paraptosis. A: Differences of logarithmic anticancer activity of the metal-free ligand to the respective copper in the indicated cell lines complex [$pIC_{50}(TSC) - pIC_{50}(Cu-TSC)$]. IC_{50} values were determined in mono- or co-culture as described in the Materials and Methods section after 72 h. **B:** Fold resistance of MES-SA/Dx5 compared to MES-SA cells against either the metal-free TSCs or the respective copper(II) complexes (Cu-TSC). **C:** Representative microscopy images of SW480 cells treated with 1 μM of the indicated metal-free TSCs for 24 h. Arrows indicate the cytoplasmic vesicles. Scale bar: 100 μm . The graph on the right shows the percentage of cytoplasmic vesicles observed after treatment of SW480 cells with 0.1 or 1 μM metal-free TSC for 24 h. Values given are mean \pm standard deviation of three areas per well of two

independent experiments. Line indicates 10% threshold of vesicle induction. **D**: Metal-free compounds inducing vesicles (threshold: 10%) at 1 μM in SW480 cells also showed a higher anticancer activity in the nanomolar range [$\text{pIC}_{50} = -\log(\text{IC}_{50})$]. Significance between groups was calculated using T-test by two-tailed t-test using GraphPad Prism software (** $p < 0.01$). Open symbols indicate nanomolar-active TSCs.

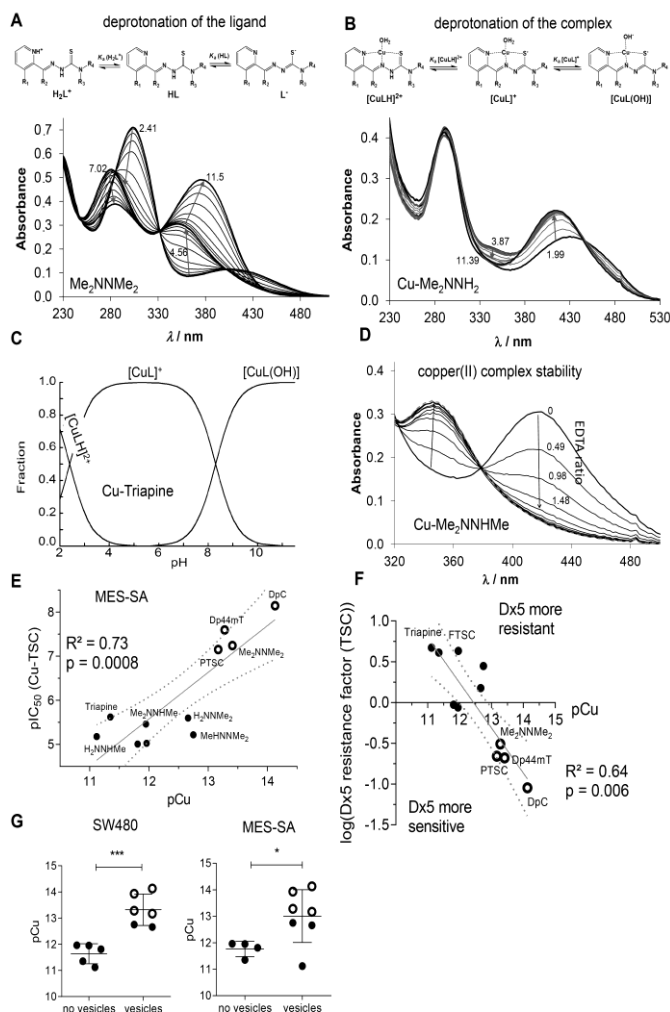


Figure 2: Higher copper(II) complex stability correlates with increased anticancer activity.

A: UV-vis spectra of Me_2NNMe_2 ($40 \mu\text{M}$) recorded at pH values between 2 and 11.9 and scheme for stepwise deprotonation of metal-free TSCs. **B:** UV-vis spectra of the copper(II) complex of Me_2NNH_2 ($25 \mu\text{M}$) recorded at pH values between 2 and 11.5 and scheme of stepwise deprotonation of TSC copper(II) complexes. **C:** Speciation curves of Cu-Triapine system depending on pH. **D:** UV-vis spectra of the copper(II) complex of Me_2NNMeH ($25 \mu\text{M}$) in the presence of EDTA at various ratios (EDTA to complex, $C_{\text{EDTA}} = 0\text{-}175 \mu\text{M}$) and the spectrum of the metal-free Me_2NNMeH (grey dashed line) at pH 5.9. **E:** Correlation of pCu [$-\log(\text{Cu(II)})$] values, representing copper(II) complex stability, to anticancer activity (pIC_{50} values) of the TSC copper complexes in MES-SA cells. R^2 and p values have been calculated using Graph Pad Prism software. **F:** Correlation of pCu to the logarithmic resistance factor

to the metal-free TSCs of MES-SA/Dx5 cells compared to parental MES-SA cells. R^2 and p values have been calculated using Graph Pad prism software. **G**: Grouping of the compounds by vesicle induction (threshold: 10%) at 1 μ M treatment metal-free ligand of SW480 for 24 h or MES-SA cells for 48 h showed a higher complex stability in vesicle-inducing TSCs. Significance between groups was calculated by two-tailed T-test using GraphPad Prism software (** $p < 0.001$, * $p < 0.05$). Open symbols indicate nanomolar-active TSCs.

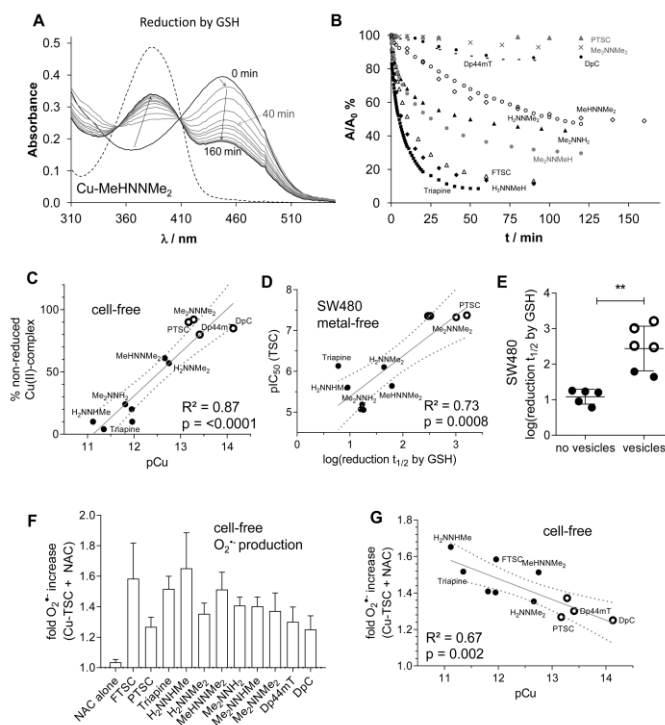


Figure 3: Cell-free reduction rate and superoxide production of copper(II) complexes and their correlation with biological activity. **A:** Time dependence of the UV-vis spectra of the MeHNNMe₂ copper(II) complex (25 μM) in the presence of 50 equivalents GSH (1.25 mM) and the spectrum of the metal-free ligand (dashed line) at pH 7.4 under O₂-free condition. **B:** Decrease of absorbance (in % A/A₀) recorded at λ_{max} of the different copper(II) TSC complexes over time at the same conditions given in **A**. Symbols: Triapine (■), H₂NNHMe (◆), FTSC (▲), Me₂NNHMe (●), Me₂NNH₂ (▲), MeHNNMe₂ (◆), H₂NNMe₂ (●), Dp44mT (–), DpC (●), Me₂NNMe₂ (x) and PTSC (▲). **C:** Correlation of pCu to the % of non-reduced copper(II) complexes calculated from GSH reduction studies. **D:** Correlations of the logarithmic reduction half-life of the TSC complexes by GSH to the anticancer activity (pIC₅₀ values) of metal-free ligands or copper(II) complexes in SW480 cells. R² and p values have been calculated using Graph Pad prism software. **E:** Grouping of the compounds by vesicle induction (threshold: 10%) at 1 μM treatment metal-free ligand for 48 h in SW480 cells showed a slower copper(II) complex reduction by GSH in vesicle-inducing TSCs. Significance between groups was calculated by two-tailed T-test using GraphPad Prism software (** p < 0.01). Open symbols indicate nanomolar-active TSCs. **F:** Fold increase of superoxide levels by 5 μM treatment of indicated TSC copper(II) complexes in the presence

of 2 mM NAC was evaluated by the cell-free NBT assay. Values given are mean \pm standard deviation of duplicates of two independent experiments. **G**: Correlation of pCu (indicating copper(II) complex stability) with superoxide production. Open symbols indicate nanomolar-active TSCs. R^2 and p values have been calculated using Graph Pad prism software.

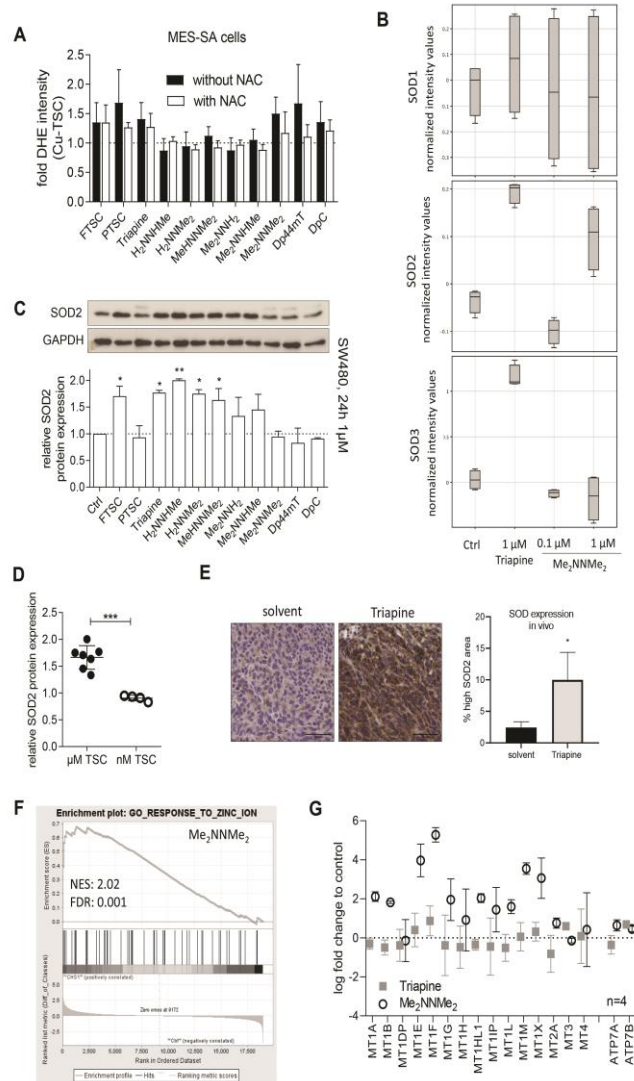


Figure 4: Upregulated redox stress signaling after TSC treatment. **A:** Intracellular superoxide production measured by flow cytometry of DHE fluorescence of MES-SA cells treated with 5 μM of indicated TSC with or without 2 mM NAC for 1 h. Values given are mean ± standard deviation of at least three independent experiments. **B:** Normalized mRNA expression values for SOD1/2/3 of SW480 cells untreated or treated with 0.1 μM Me₂NNMe₂, 1 μM Me₂NNMe₂ or 1 μM Triapine for 15 h were assessed by whole genome gene expression analysis performed with two technical replicates from two biological replicates. Normalization and annotation was performed with GeneSpring software (Agilent). **C:** Western blot analysis of SOD2 expressed by SW480 cells treated with 1 μM of the indicated TSC for 24 h. GAPDH was used as a loading control. Densitometric

quantification using ImageJ of two separate experiments is given as mean \pm standard deviation. Significance to control was calculated by one-way Anova and Dunnett's multiple comparison test using GraphPad Prism software (** $p < 0.01$, * $p < 0.05$). **D:** Micromolar-active TSC-treated SW480 cells express higher protein levels of SOD2 than nanomolar-active TSC-treated cells. Open symbols indicate nanomolar active TSCs. **E:** Female Balb/c mice bearing subcutaneous CT-26 tumors were treated with solvent (10% DMSO, $n = 4$) or Triapine (10 mg/kg, $n = 4$) p.o. for 5 consecutive days a week for two weeks. Tumor were sampled and paraffin-embedded for immunohistochemical stain of SOD2. Representative images of the stain are depicted (scalebar = 50 μm). Percent highly positive SOD2-stained area of whole tissue slides were analysed by Definiens software. Significant difference to solvent group was calculated by one-way ANOVA with Dunnett's multiple comparison test (* $p < 0.05$). **F:** GSEA from whole-genome gene expression data revealed significant enrichment in genes of the Gene Ontology term "Response to zinc ion" in SW480 cells treated with 1 μM Me_2NNMe_2 compared to untreated cells. Normalized enrichment score (NES) and false discovery rate (FDR) are given. **G:** Upregulation of metallothioneins and copper transporter ATP7A/B mainly contributed to the enrichment of the Gene Ontology term "Response to zinc ion" as seen by their individual mRNA expression levels given as mean log fold change to control \pm standard deviation.

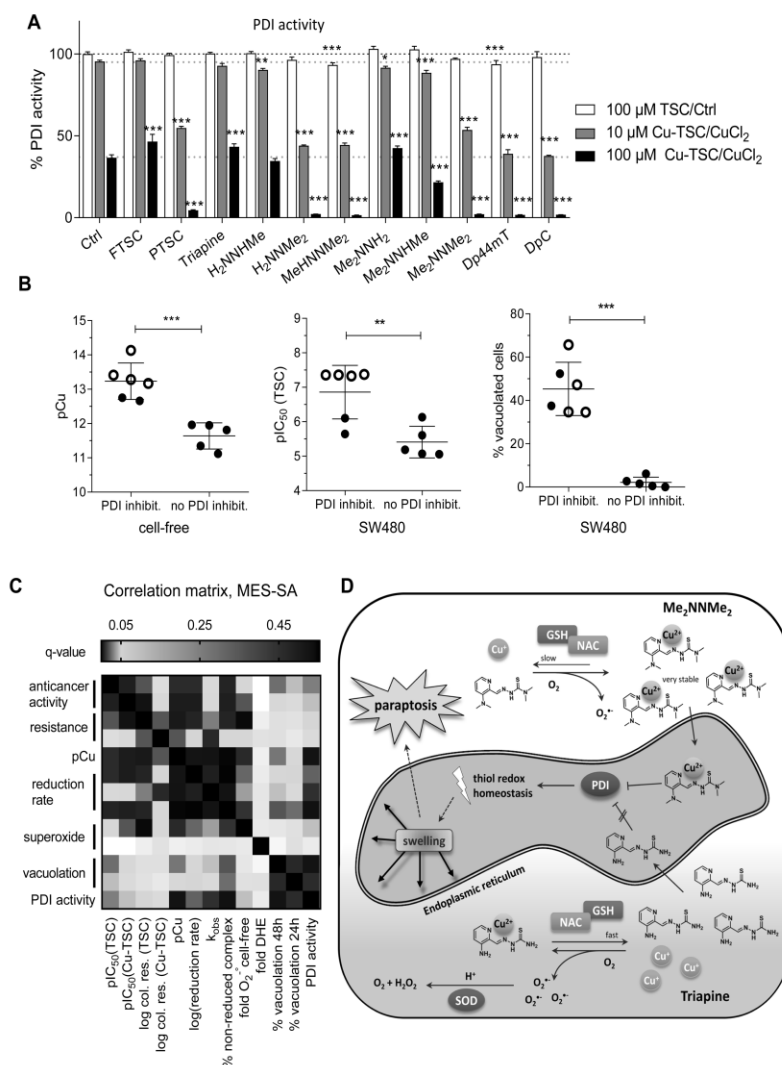


Figure 5: Inhibition of PDI by TSC copper(II) complexes. **A:** PDI activity was measured with 10 or 100 μ M of indicated TSC copper(II) complexes or copper alone using the PROTEOSTAT PDI assay kit. **B:** TSC complexes that inhibit PDI above levels of copper ions alone also showed higher pCu (indicating copper(II) complex stability), anticancer activity (in SW480 cells) and vesicle formation (in SW480 cells). Open symbols indicate nanomolar-active TSCs. **C:** Correlation matrix of measured chemical and biological parameters in MES-SA cells. P-values corrected for multiple comparisons (q-value) with an FDR of 1% are indicated with grayscale and were calculated with GraphPad Prism 8. Labels on x-axis are grouped thematically on the y-axis for a better overview. **D:** Differences in the proposed mode of action of nanomolar-active TSCs (represented by Me₂NNMe₂) and micromolar-active TSCs (represented by Triapine).

Suppl. Table 1: IC₅₀ (3 and 24 h) values of tested compounds in SW480 cells

	TSC IC ₅₀ (μM)		Cu-TSC IC ₅₀ (μM)	
	3 h	24 h	3 h	24 h
FTSC	> 25	> 25	> 25	10.39 ± 2.70
PTSC	> 25	> 25	4.43 ± 1.66	0.42 ± 0.21
Triapine	> 25	> 25	> 25	> 25
H ₂ NNHMe	> 25	> 25	> 25	> 25
H ₂ NNMe ₂	> 25	> 25	> 25	19.85 ± 3.87
MeHNNMe ₂	> 25	> 25	32.18 ± 3.01	7.32 ± 0.78
Me ₂ NNH ₂	> 25	> 25	34.15 ± 3.03	7.90 ± 1.06
Me ₂ NNHMe	> 25	> 25	15.20 ± 2.76	2.14 ± 0.33
Me ₂ NNMe ₂	> 25	> 25	6.51 ± 0.57	0.60 ± 0.11
Dp44mT	> 25	> 25	6.24 ± 0.33	0.40 ± 0.16
DpC	> 25	16.97 ± 2.15	5.03 ± 1.88	0.78 ± 0.19

Suppl. Table 1: IC₅₀ (3 and 24 h) values of tested compounds in SW480 cells

	TSC IC ₅₀ (μM)		Cu-TSC IC ₅₀ (μM)	
	3 h	24 h	3 h	24 h
FTSC	> 25	> 25	> 25	10.39 ± 2.70
PTSC	> 25	> 25	4.43 ± 1.66	0.42 ± 0.21
Triapine	> 25	> 25	> 25	> 25
H ₂ NNHMe	> 25	> 25	> 25	> 25
H ₂ NNMe ₂	> 25	> 25	> 25	19.85 ± 3.87
MeHNNMe ₂	> 25	> 25	32.18 ± 3.01	7.32 ± 0.78
Me ₂ NNH ₂	> 25	> 25	34.15 ± 3.03	7.90 ± 1.06
Me ₂ NNHMe	> 25	> 25	15.20 ± 2.76	2.14 ± 0.33
Me ₂ NNMe ₂	> 25	> 25	6.51 ± 0.57	0.60 ± 0.11
Dp44mT	> 25	> 25	6.24 ± 0.33	0.40 ± 0.16
DpC	> 25	16.97 ± 2.15	5.03 ± 1.88	0.78 ± 0.19

Suppl. Table 3: IC₅₀ (24 h) values of tested compounds in MES-SA and MES-SA/Dx5 cells.

	TSC IC ₅₀ (μM)		Cu-TSC IC ₅₀ (μM)	
	MES-SA	MES-SA/Dx5	MES-SA	MES-SA/Dx5
FTSC	> 25	> 25	> 25	> 25
PTSC	1.98 ± 0.23	> 25	1.45 ± 0.37	> 25
Triapine	> 25	> 25	> 25	> 25
H ₂ NNHMe	> 25	> 25	> 25	> 25
H ₂ NNMe ₂	> 25	> 25	> 25	> 25
MeHNNMe ₂	> 25	21.55 ± 5.14	19.78 ± 2.61	14.74 ± 1.45
Me ₂ NNH ₂	> 25	24.99 ± 0.33	> 25	26.47 ± 0.74
Me ₂ NNHMe	> 25	> 25	> 25	> 25
Me ₂ NNMe ₂	> 25	> 25	> 25	13.54 ± 0.91
Dp44mT	3.04 ± 0.24	13.33 ± 0.94	1.29 ± 0.46	7.43 ± 0.57
DpC	11.43 ± 0.61	> 25	5.93 ± 0.59	16.37

Suppl. Table 4: IC₅₀ (144 h) values of tested compounds in MES-SA and MES-SA/Dx5 cells

	TSC IC ₅₀ (μM)		Cu-TSC IC ₅₀ (μM)	
	MES-SA	MES-SA/Dx5	MES-SA	MES-SA/Dx5
FTSC	1.43 ± 0.18	9.00 ± 0.96	10.66 ± 0.55	3.93 ± 0.85
PTSC	0.0365 ± 0.0089	0.0163 ± 0.0026	0.0268 ± 0.0096	0.0129 ± 0.0025
Triapine	0.53 ± 0.07	2.84 ± 0.38	1.94 ± 0.32	20.49 ± 2.55
H ₂ NNHMe	0.71 ± 0.10	4.91 ± 0.28	4.13 ± 0.41	32.06 ± 2.66
H ₂ NNMe ₂	0.41 ± 0.09	0.87 ± 0.21	2.40 ± 0.27	4.44 ± 0.06
MeHNNMe ₂	1.04 ± 0.05	1.15 ± 0.13	5.06 ± 0.79	1.59 ± 0.30
Me ₂ NNH ₂	4.02 ± 0.43	3.97 ± 0.57	10.41 ± 0.47	3.09 ± 0.14
Me ₂ NNHMe	2.76 ± 0.34	2.19 ± 0.35	2.83 ± 0.54	1.02 ± 0.04
Me ₂ NNMe ₂	0.0084 ± 0.0024	0.0028 ± 0.0003	0.0131 ± 0.0037	0.0034 ± 0.0008
Dp44mT	0.0127 ± 0.0034	0.0040 ± 0.0007	0.0058 ± 0.0013	0.0021 ± 0.0005
DpC	0.0052 ± 0.0014	0.0023 ± 0.0006	0.0032 ± 0.0008	0.0013 ± 0.0003

Suppl. Table 5: Calculated λ_{\max} (nm) and ϵ ($M^{-1}cm^{-1}$) values of the ligand species in the different protonation states .

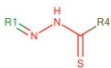
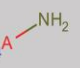
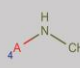
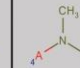
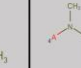
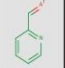
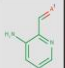
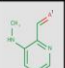

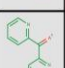
ligand	medium	λ_{\max} (nm) / ϵ ($M^{-1}cm^{-1}$)		
		H_2L^+	HL	L^-
Triapine	H ₂ O	394 / 18860	358 / 15000	368 / 17450
H ₂ NNHMe	H ₂ O	390 / 16386	354 / 12899	382 / 14841
H ₂ NNMe ₂	H ₂ O	390 / 17300	360 / 12460	378 / 18875
MeHNNMe ₂	H ₂ O	408 / 15290	382 / 11230	394 / 17810
Me ₂ NNH ₂	H ₂ O	412 / 8140	348 / 9450	366 / 12830
Me ₂ NNHMe	H ₂ O	413 / 10240	349 / 12200	378 / 16930
Me ₂ NNMe ₂	H ₂ O	411 / 2900	350 / 7793	377 / 12990
FTSC	H ₂ O	342 / 22003	310 / 22924	342 / 17187
PTSC	H ₂ O	334 / 17323	306 / 16104	354 / 14966
Dp44mT	H ₂ O	344 / 16635	324 / 16000	376 / 13370
DpC	5% DMSO	346 / 17970	328 / 15040	382 / 10750
DpC	30% DMSO	348 / 18620	328 / 17300	388 / 15140
Triapine *	30% DMSO	402 / 20600	368 / 15600	376 / 17200
H ₂ NNMe ₂ *	30% DMSO	398 / 18200	366 / 13600	384 / 20700

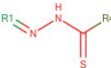
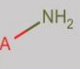
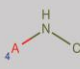
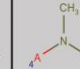
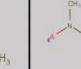
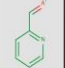
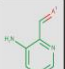
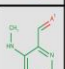

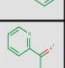
* Data taken from Ref. (6)

Suppl. Table 6: pK_a values of the TSC copper(II) complexes determined by spectrophotometric titrations and conditional ($\log\beta'$) stability constants for $[\text{CuL}]^+$ species at pH 5.90 determined via EDTA displacement reaction .

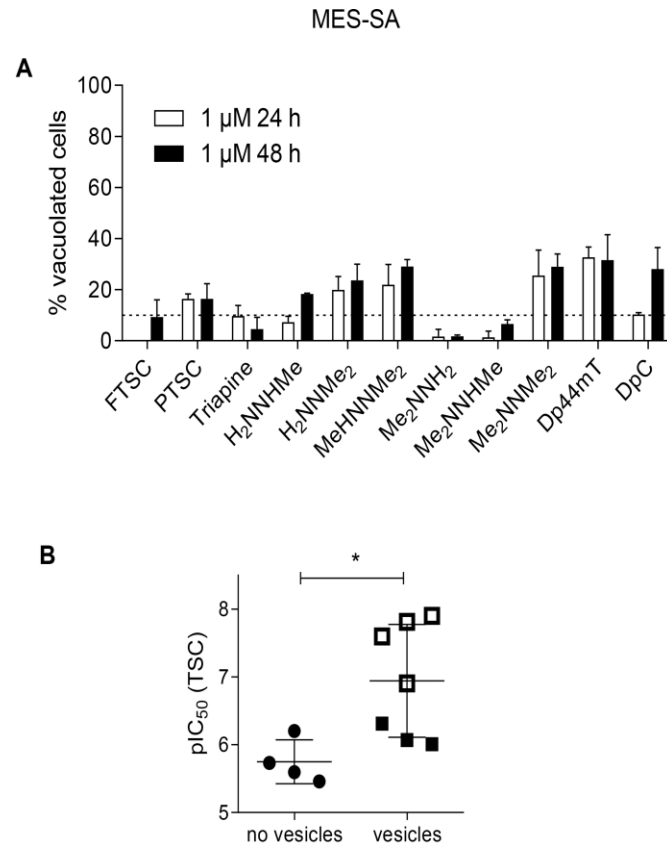
ligand	medium	pK_a $[\text{CuLH}]^{2+}$	pK_a $[\text{CuL}]^+$	$\log\beta'_{5.9}$ $[\text{CuL}]^+$
Triapine *	H ₂ O	2.51	8.64	12.88
H₂NNHMe	H ₂ O	2.54±0.01	8.62±0.01	12.58±0.02
H₂NNMe₂	H ₂ O	2.51±0.02	8.65±0.07	14.12±0.01
MeHNNMe₂	H ₂ O	2.64±0.02	8.19±0.02	14.15±0.03
Me₂NNH₂	H ₂ O	2.31±0.02	8.53±0.01	13.27±0.03
Me₂NNHMe	H ₂ O	2.57±0.02	8.11±0.02	13.35±0.02
Me₂NNMe₂	H ₂ O	2.51±0.01	8.78±0.01	14.72±0.07
FTSC	H ₂ O	2.08±0.02	8.70±0.04	13.44±0.07
PTSC	H ₂ O	2.09±0.01	8.56±0.01	14.64±0.01
Dp44mT	H ₂ O	2.34±0.02	8.79±0.03	14.89±0.01
DpC	5% DMSO	–	–	–
DpC	30% DMSO	2.13±0.03	9.46±0.02	11.67±0.02 †
DpC ‡	H ₂ O	2.45	8.36	–
Triapine §	30% DMSO	2.34	9.67	–
H₂NNMe₂ §	30% DMSO	1.93	9.49	–

* Data taken from Ref. (22). † $\log\beta'_{5.90} = 10.19 \pm 0.04$ for the Cu(II)-EDTA complex in the 30% (w/w) DMSO/H₂O mixture was determined via Triapine displacement reaction. ‡ Estimated values from pK_a values of the complexes measured in the 30% (w/w) DMSO/H₂O mixture using the slopes of the pK_a vs. $1/\epsilon_r$ curves of Cu(II) complexes of Triapine and H₂NNMe₂. § Data taken from Ref. (6)

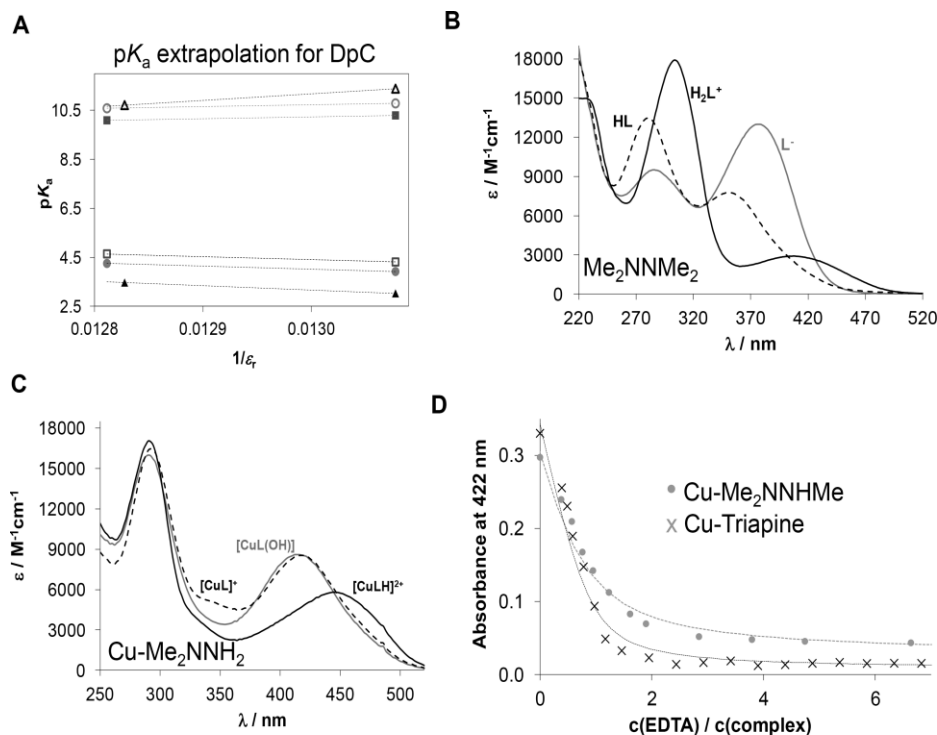
											
72h											
		FTSC				PTSC				pIC50	IC50
		5.73	5.09	5.17	5.28	6.90	7.54	n.tox.	not toxic		
	Dx5	5.03	5.37	5.35	5.77	7.15	7.62	4.50	31.6μM		
		Triapine		H2NNMeH		H2NNMe2		5.00	10μM		
	Dx5	6.20	5.59	6.07	5.40	6.31	6.13	5.50	3.2μM		
						MeHNNMe2		6.50	316.2nM		
	Dx5	5.78	5.08	5.65	5.23	6.01	n.tox.	7.00	100nM		
		Me2NNH2		Me2NNHMe		Me2NNMe2		8.00	10nM		
	Dx5	5.46	5.49	5.59	5.66	7.90	8.41	8.50	3.16nM		
						Dp44mT		8.00	10nM		
	Dx5	5.01	5.49	5.46	5.95	7.60	8.14	9.00	1nM		
pIC50s						Dp44mT				DpC	
MES-SA						7.60	8.25	7.81	8.51		
CuL_MESS/CuL_Dx5						7.24	8.42	8.15	8.90		

											
144h											
		FTSC				PTSC				pIC50	IC50
		5.85	5.05	5.19	5.28	7.45	7.79	n.tox.	not toxic		
	Dx5	4.97	5.42	5.24	5.78	7.60	7.90	4.50	31.6μM		
		Triapine		H2NNMeH		H2NNMe2		5.00	10μM		
	Dx5	6.28	5.55	6.15	5.31	6.40	6.07	5.50	3.2μM		
						MeHNNMe2		6.50	316.2nM		
	Dx5	5.89	5.04	5.79	5.28	5.99	n.tox.	7.00	100nM		
		Me2NNH2		Me2NNHMe		Me2NNMe2		8.00	10nM		
	Dx5	5.40	5.41	5.56	5.67	8.09	8.56	8.50	3.16nM		
						Dp44mT		8.00	10nM		
	Dx5	4.98	5.51	5.56	5.99	7.90	8.47	9.00	1nM		
pIC50s						Dp44mT				DpC	
MES-SA						7.91	8.40	8.30	8.65		
CuL_MESS/CuL_Dx5						8.25	8.69	8.51	8.89		

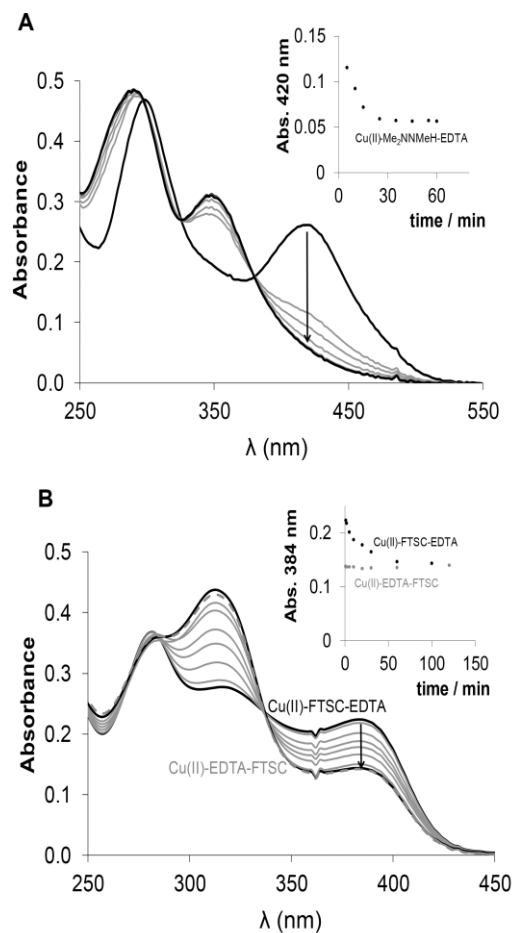
Suppl. Figure 1: Structure activity relationship matrix (SARM) showing the negative logarithmic IC₅₀ values (pIC₅₀) of MES-SA and MES-SA/Dx5 cells treated with our TSC panel as metal-free ligand or copper(II) complex for 72 and 144 h.



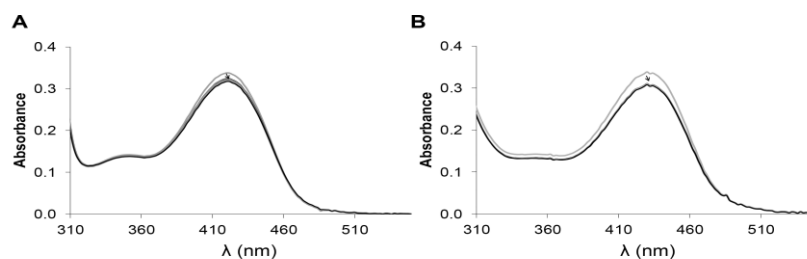
Suppl. Figure 2: A: Percentage of cytoplasmic vesicles observed after treatment of MES-SA cells with 1 μM metal-free TSC in medium containing 1% serum for 24 h or 48 h. Values given are mean \pm standard deviation of three areas per well. Line indicates 10% threshold of vesicle induction. **B:** Metal-free compounds inducing vesicles (threshold: 10%) at 1 μM in MES-SA cells also showed a higher anticancer activity ($\text{pIC}_{50} = -\log_{10}(\text{IC}_{50})$) in the nanomolar range. Significance between groups was calculated by two-tailed t-test using GraphPad Prism software (* $p < 0.05$)



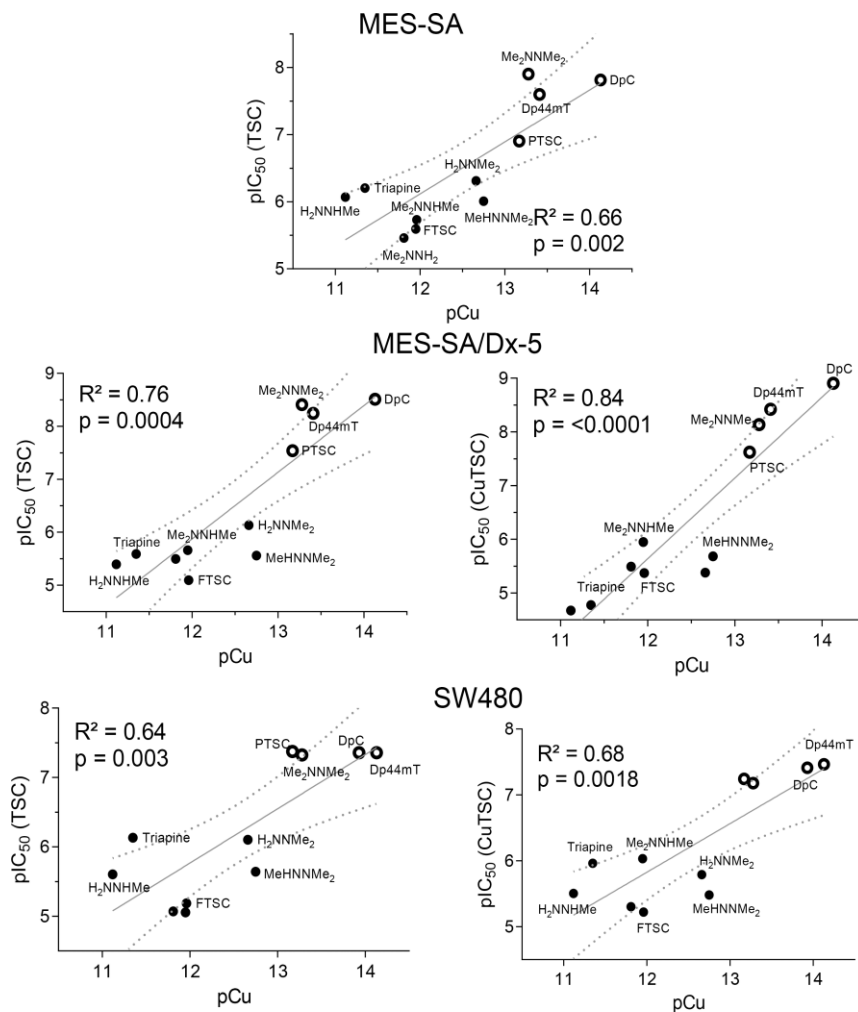
Suppl. Figure 3: **A:** Correlation diagram for the pK_a values measured at various DMSO content plotted against the $1/\epsilon_r$ values of the solvent medium for Triapine (\bullet ; \circ), H_2NNMe_2 (\blacksquare ; \square) and DpC (\blacktriangle ; \triangle). **B:** Calculated individual absorption spectra from a measured UV-vis spectra of Me_2NNMe_2 ($40 \mu M$) recorded at pH values between 2 and 11.9. **C:** Calculated individual absorption spectra from a measured UV-vis spectra of the copper(II) complex of Me_2NNH_2 recorded at pH values between 2 and 11.9. **D:** Absorbance values recorded for copper(II)- Me_2NNHMe -EDTA (\bullet) and copper(II)-Triapine-EDTA (\times) systems at 422 nm with the simulated curves (dashed lines) at the various complex-to-EDTA ratios.



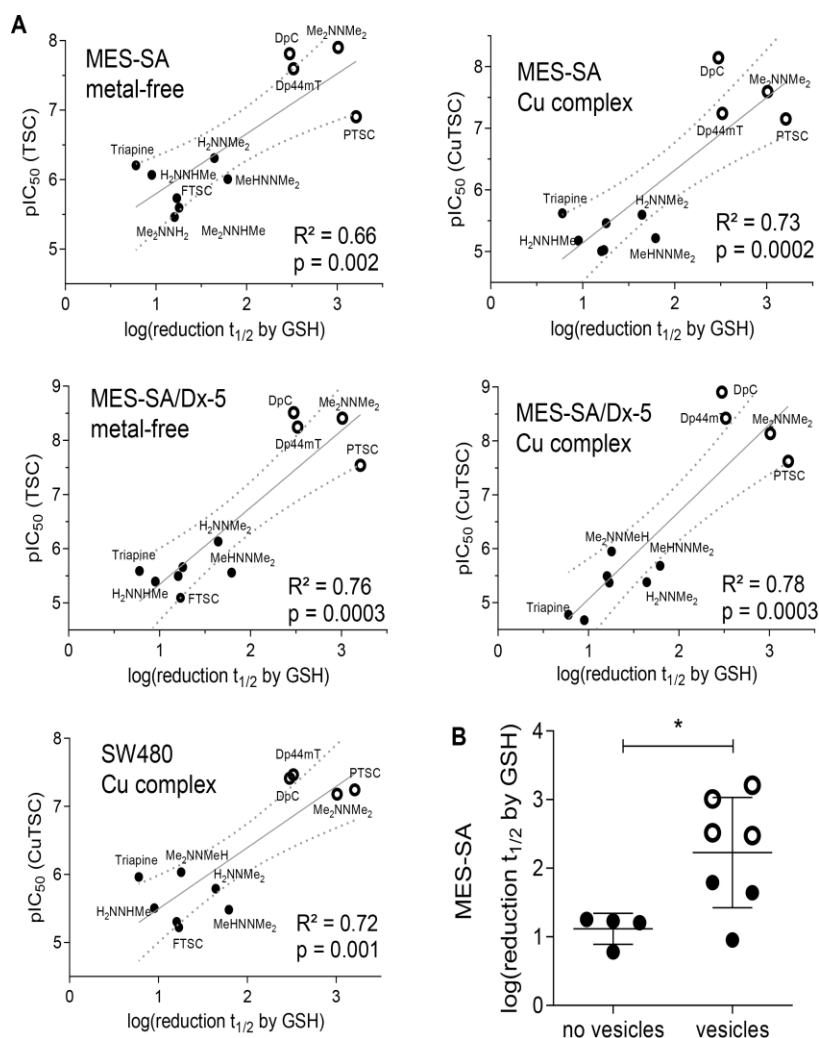
Suppl. Figure 4: Time-dependence of UV-vis spectra of the copper(II) complex of Me₂NNMeH (A) and FTSC (B) in the presence of EDTA at 1:1 complex-to-EDTA ratio. Inserted figures show the absorbance changes at 420 nm (A) and at 384 nm (B) in dependence of time. The green dashed line in fig. B shows the absorbance spectrum recorded for the reverse reaction when 1 eq FTSC ligand was added to the copper(II)-EDTA complex after 60 min waiting time and the green symbols (●) show the changes of the absorbance values at 384 nm in time. ($c_{\text{copper(II)}} = 25 \mu\text{M}$, $c_{\text{ligand}} = 25 \mu\text{M}$, $c_{\text{EDTA}} = 25 \mu\text{M}$, pH 5.9).



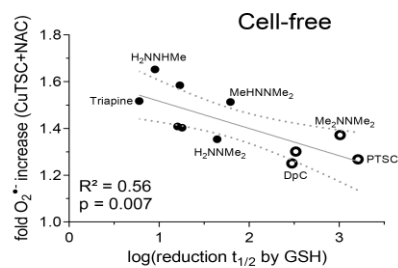
Suppl. Figure 5: Time-dependence of UV-vis spectra of the copper(II) complex of Triapine (a) and H_2NNMe_2 (b) in the presence of 50 eq ascorbate at pH 7.4 under O_2 -free condition. The green line shows the spectrum of the sample before mixing the reagents. ($C_{\text{copper(II)}} = 25 \mu\text{M}$, $C_{\text{ligand}} = 25 \mu\text{M}$, $C_{\text{ascorbate}} = 1250 \mu\text{M}$, pH 7.4 (HEPES))



Suppl. Figure 6: Correlation of pCu values, representing copper(II) complex stability, to anticancer activity (pIC₅₀ values) of the metal-free TSCs or the copper(II) complexes in MES-SA cells, MES-SA/Dx5 or SW480 cells. Correlation with Cu-TSC in MES-SA cells is shown in Figure 2E. R² and p values have been calculated using Graph Pad prism software.



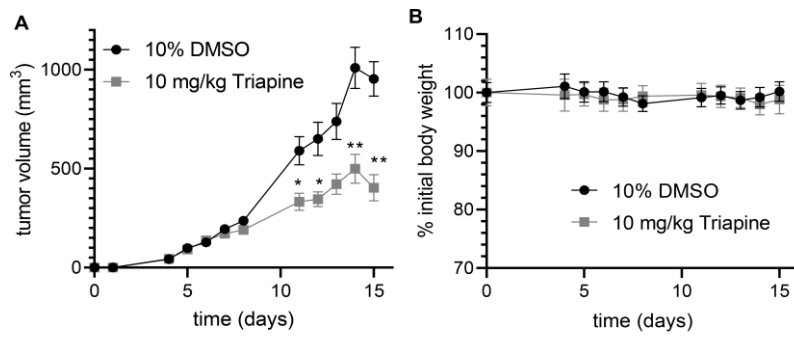
Suppl. Figure 7: A: Correlation of the logarithmic reduction half-life of the TSC copper(II) complexes reduced by GSH to anticancer activity (pIC_{50} values) of the metal-free TSCs or the copper(II) complexes in MES-SA cells, MES-SA/Dx5 or SW480 cells. R^2 and p values have been calculated using Graph Pad prism software. **B:** Grouping of the compounds by vesicle induction (threshold: 10%) at 1 μ M treatment metal-free ligand for 24 h in MES-SA cells showed a slower copper(II) complex reduction by GSH in vesicle-inducing TSCs. Significance between groups was calculated by two-tailed T-test using GraphPad Prism software (* $p < 0.05$). Open symbols indicate nanomolar-active TSCs.



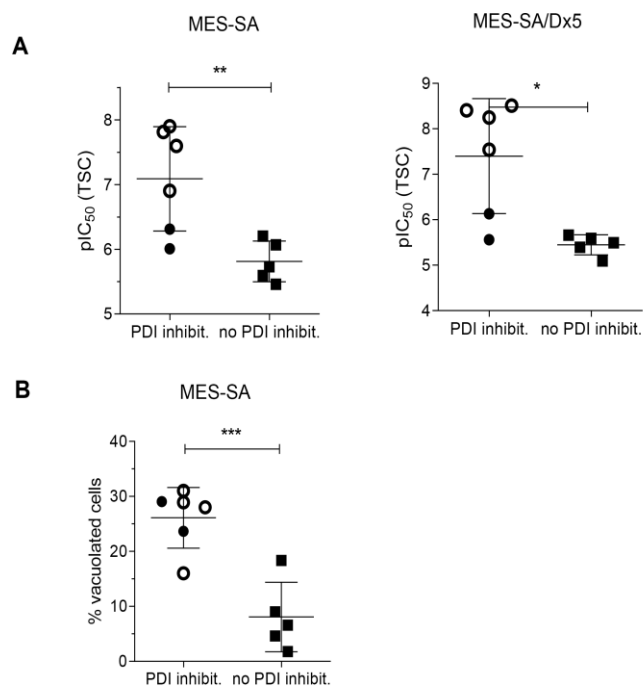
Suppl. Figure 8: Correlation of logarithmic reduction half-life of the TSC copper(II) complexes reduced by GSH to the superoxide production by the TSC copper complexes in the presence of NAC. R^2 and p values have been calculated using Graph Pad prism software.

GO_REGULATION_OF_RESPONSE_TO_OXIDATIVE_STRESS								
TSC vs ctrl	rank	size	ES	NES	nom p-val	FDR q-val	FWER p-val	rank at max
Me ₂ NNMe ₂	678	59	0.49	1.49	0.022	0.101	1.000	2697
Triapine	988	59	0.39	1.25	0.142	0.347	1.000	2664

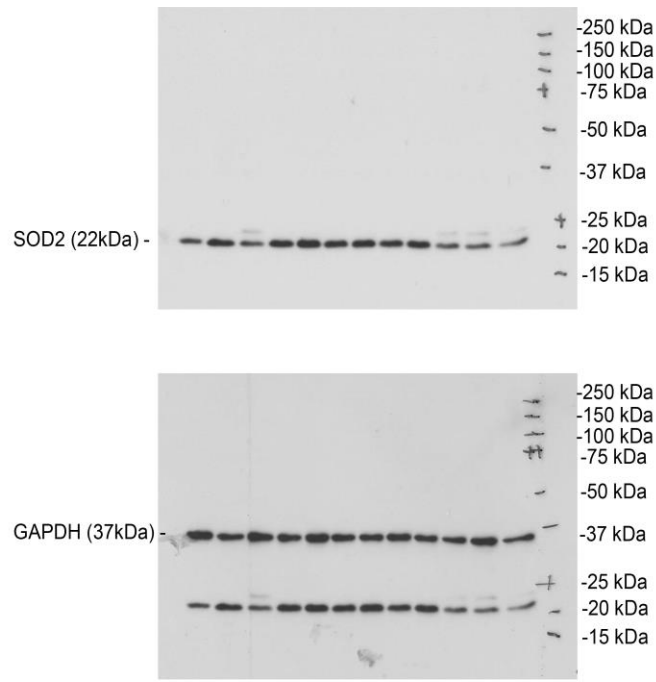
Suppl. Figure 9: Gene set enrichment analysis of Gene Ontology terms revealed no significant upregulation of response to oxidative stress gene sets after Me₂NNMe₂ or Triapine treatment of SW480 cells, as depicted by the high FDR and FWER values of the most relevant gene set „regulation of response to oxidative stress“.



Suppl. Figure 10: Female Balb/c mice bearing subcutaneous CT-26 tumors were treated with solvent (10% DMSO) or Triapine (10 mg/kg), p.o. for 5 consecutive days a week for two weeks. **A:** Tumor size was assessed regularly by caliper measurement. Tumor volumes (means \pm standard errors of the mean, SEM), calculated using the formula: length \times width²/2. Significance to solvent group was calculated by mixed-effect model (REML) with Dunnett's multiple comparison test (** $p < 0.01$). **B:** Body weight changes in percent to initial body weight is given as means \pm standard errors of the mean, SEM.



Suppl. Figure 11: TSC complexes that inhibit PDI above levels of copper ions alone also showed higher anticancer activity in MES-SA or MES-SA/Dx5 cells (**A**) and vesicle formation in MES-SA cells (**B**).



Suppl. Western: Whole film of Western blot analysis shown in Figure 4 of the main manuscript.